PLOS PATHOGENS

RESEARCH ARTICLE

Salmonella Typhimurium impairs glycolysis-mediated acidification of phagosomes to evade macrophage defense

Saray Gutiérrez[1], Julia Fischer[1,2,3], Raja Ganesan[4], Nina Judith Hos[1,3,5¤a], Gökhan Cildir[4], Martina Wolke[5], Alberto Pessia[6], Peter Frommolt[7¤b], Vincenzo Desiderio[8], Vidya Velagapudi[6], Nirmal Robinson[1,4,5]*

1 Cologne Excellence Cluster on Cellular Stress Responses in Aging-Associated Diseases (CECAD), University of Cologne, Cologne, Germany, **2** First Department of Internal Medicine, University of Cologne, Cologne, Germany, **3** German Center for Infection Research (DZIF), Partner Site Bonn-Cologne, Germany, **4** Centre for Cancer Biology, University of South Australia, Adelaide, Australia, **5** Institute for Medical Microbiology, Immunology and Hygiene, University of Cologne, Cologne, Germany, **6** Metabolomics Unit, Institute for Molecular Medicine Finland FIMM, Helsinki, Finland, **7** Bioinformatics Facility, CECAD, University of Cologne, Cologne, Germany, **8** Department of Precision Medicine, University of Campania "Luigi Vanvitelli", Naples, Italy

¤a Current address: London School of Hygiene and Tropical Medicine, Department for Clinical Research, London, United Kingdom
¤b Current address: Institute of Human Genetics, University Medical Center Hamburg-Eppendorf
* nirmal.robinson@unisa.edu.au

Citation: Gutiérrez S, Fischer J, Ganesan R, Hos NJ, Cildir G, Wolke M, et al. (2021) *Salmonella* Typhimurium impairs glycolysis-mediated acidification of phagosomes to evade macrophage defense. PLoS Pathog 17(9): e1009943. https://doi.org/10.1371/journal.ppat.1009943

Editor: Nina R. Salama, Fred Hutchinson Cancer Research Center, UNITED STATES

Received: March 29, 2021

Accepted: September 7, 2021

Published: September 23, 2021

Data Availability Statement: All relevant data are within the manuscript and its Supporting Information files.

Funding: NR received funding from CECAD D3, Deutsche Forschungsgemeinschaft (DFG), from SFB670 (N31) Deutsche Forschungsgemeinschaft (DFG); from Koeln Fortune and from University of South Australia (UniSA). SG was supported by funds from DFG; NJH and JF were supported by funds from German Center for Infection Research (DZIF). RG was supported by funds from UniSA.

Abstract

Regulation of cellular metabolism is now recognized as a crucial mechanism for the activation of innate and adaptive immune cells upon diverse extracellular stimuli. Macrophages, for instance, increase glycolysis upon stimulation with pathogen-associated molecular patterns (PAMPs). Conceivably, pathogens also counteract these metabolic changes for their own survival in the host. Despite this dynamic interplay in host-pathogen interactions, the role of immunometabolism in the context of intracellular bacterial infections is still unclear. Here, employing unbiased metabolomic and transcriptomic approaches, we investigated the role of metabolic adaptations of macrophages upon *Salmonella enterica* serovar Typhimurium (*S*. Typhimurium) infections. Importantly, our results suggest that *S*. Typhimurium abrogates glycolysis and its modulators such as insulin-signaling to impair macrophage defense. Mechanistically, glycolysis facilitates glycolytic enzyme aldolase A mediated v-ATPase assembly and the acidification of phagosomes which is critical for lysosomal degradation. Thus, impairment in the glycolytic machinery eventually leads to decreased bacterial clearance and antigen presentation in murine macrophages (BMDM). Collectively, our results highlight a vital molecular link between metabolic adaptation and phagosome maturation in macrophages, which is targeted by *S*. Typhimurium to evade cell-autonomous defense.

The funders had no role in study design, data collection and analysis, decision to publish, or preparation of the manuscript.

Competing interests: The authors have declared that no competing interests exist.

Author summary

Macrophages undergo metabolic adaptations when they respond to invading pathogens. On the other hand, pathogens are also known to disrupt metabolic pathways to evade immune defense. In this study, we have employed metabolomics and transcriptomics to unravel that *S*. Typhimurium abrogates glycolysis and the modulators of glycolysis such as insulin-signaling. Downregulation of glycolysis leads to reduced acidification of phagosomes resulting in impaired bacterial clearance and antigen presentation. Furthermore, we provide evidence that induction of glycolysis facilitates v-ATPase assembly and the acidification of phagosomes by mobilizing aldolase to the v-ATPase complex. Our results highlight a previously unknown molecular link between metabolism and phagolysosome, which is targeted by *S*. Typhimurium to evade cell-autonomous defense.

Introduction

Macrophages are sentinel immune cells playing pivotal roles in the host defense. They not only engulf and degrade the pathogens, but also secrete cytokines and present antigens to T cells to mount an effective adaptive immune response [1]. Several pathogens such as *Salmonella enterica* serovar Typhimurium (*S*. Typhimurium) are restrained in phagosomes after being quickly phagocytosed by macrophages. However, *S*. Typhimurium also has evolved mechanisms to evade the hostile milieu of lysosomes and induce inflammatory cell death in macrophages. We have previously shown that *S*. Typhimurium induces type I interferon (IFN-I)-dependent and receptor-interacting serine/threonine-protein kinase 3 (RIP3)-mediated necroptosis in macrophages [2]. It is also known that pro-inflammatory, necrotic cell death is associated with energy deficiency and metabolic instability in the cells [3]. For instance, transfer of IFN-I receptor (IFNAR)-deficient or RIP3 kinase-deficient macrophages (that are cell death resistant) to wild type (WT) mice promotes better control of the pathogen implying that metabolically stable macrophages are more efficient in the control of pathogens [2].

A balanced immune response and metabolic homeostasis against invading pathogens are vital. Because substantial amount of energy is consumed when cells respond to immune stimuli, it is essential that they metabolically adapt to the demand [4]. Studies have highlighted the metabolic adjustments macrophages and dendritic cells undergo upon toll like receptor 4 (TLR4) activation with lipopolysaccharide (LPS) [5, 6]. It has also been suggested that classically activated macrophages (M1), which respond readily to bacterial infections, derive their energy predominantly through glycolysis. On the other hand, alternatively activated macrophages (M2), which help in maintaining tissue homeostasis, obtain their energy mainly through oxidative phosphorylation (OXPHOS) [7, 8]. Notably, metabolic intermediates arising from different metabolic pathways also significantly modulate the inflammatory response in immune cells. For instance, metabolites such as dimethyl fumarate (DMF) a derivative of fumarate and itaconate have been found to modulate the innate and adaptive immune responses [9, 10]. Similarly, tricarboxylic-acid (TCA) cycle intermediate succinate also modulates inflammation through Hypoxia-inducible factor 1-alpha (HIF-1α) in M1 macrophages [11]. Thus, there is a dynamic crosstalk between metabolic intermediates and innate immune responses. Pathogens such as *S*. Typhimurium could also target this crosstalk and impair the metabolic homeostasis in macrophages. It has been reported that *S*. Typhimurium persists in M2 macrophages in a long-term infection model by sustaining fatty acid metabolism [12]. Furthermore, *S*. Typhimurium also depend on its glycolysis machinery for survival in macrophages [13]. We had also reported that the pathogen targets energy sensors such as AMPK and Sirtuin 1 for lysosomal degradation [14]. More recently, we had shown that *S*. Typhimurium

enhances leptin signaling to evade lysosomal degradation in macrophages [15]. However, the implications of the metabolic pathways in macrophage defense against invading pathogens are largely unknown.

To understand the metabolic perturbations induced by *S*. Typhimurium, we performed an integrative metabolomics and transcriptomics analysis on murine bone marrow derived macrophages (BMDM) infected with *S*. Typhimurium. This combined omics approach has revealed that glycolysis and its associated signaling pathways, such as insulin signaling facilitating glycolysis, are significantly downregulated upon *S*. Typhimurium infection. Furthermore, we show that downregulation of glycolysis by direct chemical inhibition or by genetically disrupting insulin-signaling in myeloid cells leads to elevated bacterial burden and impaired antigen presentation as a result of reduced acidification of phagosomes. Importantly, we demonstrate that glycolysis regulates the assembly of vacuolar-type H^+-ATPase complex (v-ATPase) and hence the acidification of phagosomes and glycolytic enzyme aldolase A critically regulates this process. Overall, our findings suggest that the Warburg-like-effect observed in macrophages upon infection is critical for the phagosome/lysosome-mediated clearance of pathogens. Moreover, pathogens such as *S*. Typhimurium have evolved strategies to disrupt this immunometabolic homeostasis in macrophages.

Results

S. Typhimurium infection promotes metabolic reprogramming in macrophages

To comprehensively characterize the metabolic alterations caused by *S*. Typhimurium infection, we carried out mass spectrometric analysis of 100 metabolites in bone marrow-derived macrophages (BMDMs) infected with *S*. Typhimurium for 2h. As depicted in the PLSDA plot (**S1A Fig**) and in the heat map analysis of metabolites (**Fig 1A** for top-25 altered metabolites, **S1B Fig** for all metabolites analyzed), *S*. Typhimurium-infected macrophages presented a distinct metabolic profile when compared to uninfected (UI) controls. Metabolic pathway enrichment analysis revealed that carbohydrate-metabolism, which provides pyruvate for mitochondrial metabolism, and insulin signaling, which regulates glycolysis, were among the highly enriched pathway components upon *S*. Typhimurium infection (**Fig 1B**). Energy metabolites such as NAD+ was also highly down regulated upon *S*. Typhimurium infection (**S1C Fig**).

Complementary to this metabolite analysis, we also performed RNA-sequencing (RNA-seq) in BMDMs infected with *S*. Typhimurium at the same time point (2h). Consistent with the decrease in metabolites of glycolysis, RNA-seq data from BMDMs showed that levels of genes involved in carbohydrate metabolism and insulin signaling were significantly downregulated (**Figs 1C**, **1D** and **S1D**). Western blot analysis further confirmed that the expression levels of insulin receptor (IR) and its downstream target phosphorylated glycogen synthase kinase 3 (p-GSK3) were reduced upon *S*. Typhimurium infection (**S1E and S1F Fig**). In contrast, negative regulators of insulin signaling such as suppressors of cytokine signaling (SOCS) [16] and PTEN signaling pathway components [17] were up regulated (**Fig 1C and 1D**). Thus, metabolomics and transcriptomics together indicate that *S*. Typhimurium infection downregulates glycolysis and insulin-signaling that facilitates glycolysis.

Virulence dependent inhibition of glycolysis in *S*. Typhimurium infected macrophages

Macrophages are known to undergo a switch in metabolism from OXPHOS to glycolysis upon various extracellular stimuli [18]. However, the metabolic changes that occur upon

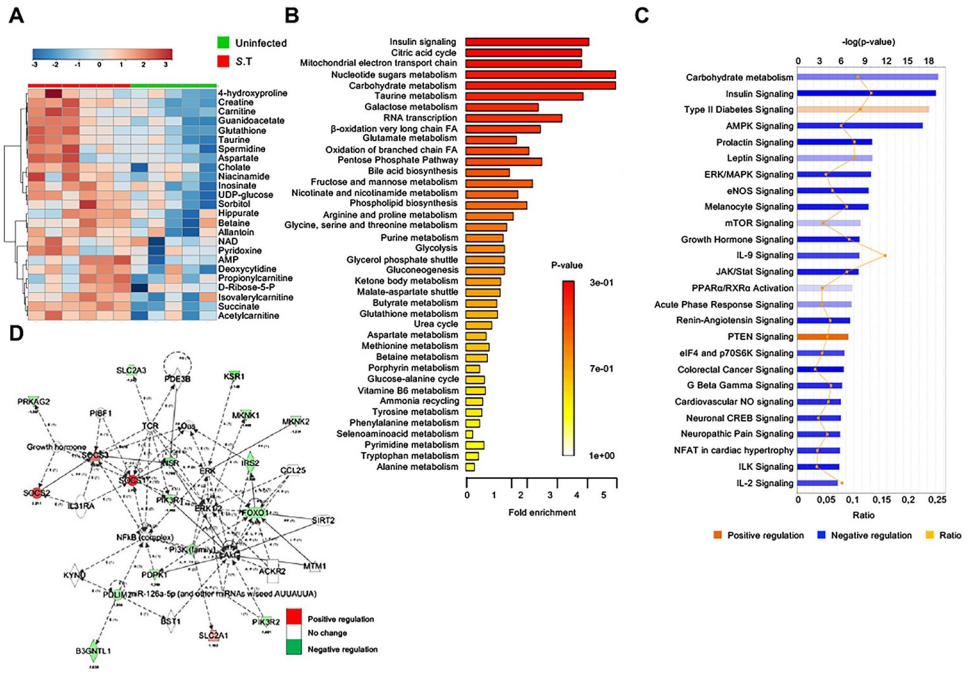

Fig 1. *S.* Typhimurium infection promotes metabolic reprogramming in macrophages. (A) Heatmap representation of 2-way hierarchical clustering of top-25 altered metabolites in BMDMs upon S. Typhimurium infection (2 h post-infection (p.i.) (n = 6) compared to uninfected controls (n = 5). **(B)** Metabolic pathway enrichment analysis of metabolomics data from S. Typhimurium-infected BMDMs (2 h p.i) compared to uninfected controls. **(C)** Ingenuity pathway analysis of genes differentially expressed in RNA-seq data from S. Typhimurium-infected BMDMs (2h p.i) compared to uninfected controls (n = 3). **(D)** Relative expression of genes from the insulin-signaling pathway in *S.* Typhimurium-infected BMDMs (2h p.i.) normalized to uninfected controls (n = 3).

https://doi.org/10.1371/journal.ppat.1009943.g001

intracellular bacterial infections are less understood. To show that glycolysis is indeed targeted by *S.* Typhimurium, we specifically analyzed the metabolites derived from glycolysis. This analysis confirmed that most of the metabolites generated upon breakdown of glucose were decreased, indicating that glucose flux was reduced upon infection with *S.* Typhimurium (**Figs 2A** and **S2A**). Consistently, *S.* Typhimurium infection of macrophages resulted in a decline in extracellular acidification rate (ECAR) at 4h, indicating reduced glycolytic flux, a phenomenon that was not observed upon LPS treatment (**Fig 2B**). Moreover, western blot analysis showed that the expression of Glut1, the main glucose transporter in macrophages [19], was significantly increased early upon infection (0.5-2h) followed by a decline during the later phase of infection (4h) (**Fig 2C**). Although, *S.* Typhimurium induced cell death was not significantly higher at 4h compared to 2h (**S2B Fig**). In line with this, the levels of glucose-sensitive transcription factor MondoA and HIF-1α were also transiently up regulated (0.5-2h) and then down regulated over time (4h) (**Fig 2D and 2E**). Importantly, the change in the levels of Glut1 and the glucose-responsive transcription factors also correlated with the glucose uptake. Uptake of fluorescent glucose analogue 2-NBDG immediately upon infection was increased followed by a steady decline during the course of *S.* Typhimurium infection (**Fig 2F**). Our transcriptomics analysis revealed that majority of the glycolytic genes were down regulated upon *S.* Typhimurium infection in comparison to uninfected controls (**S2C Fig**). Despite an increase in glucose intake during the early phase of infection, the glycolytic metabolites were declined. Therefore, it is conceivable that *S.* Typhimurium actively blocks the proportionate up regulation of genes that are required to regulate the glycolytic flux.

Next, we asked if the down regulation of glycolysis is a pathogenic mechanism of *S*. Typhimurium. Importantly, we observed that infection with heat-killed *S*. Typhimurium did not decrease the uptake of 2-NBDG (S2D Fig). To gain further insights into the virulence-dependent regulation of macrophage glycolysis by *S*. Typhimurium, we investigated the ability of two different *S*. Typhimurium mutants (known as *ssrB* and *invA*) to modulate the glycolytic response upon infection. SsrB is a *Salmonella* pathogenicity island (SPI)-2 encoded transcriptional regulator, which positively controls SPI-2 genes and represses SPI-1 genes upon entry into the cells [20] and *invA* mutant is known to be impaired in its ability to invade epithelial cells [21], but enters the macrophage by an inv locus independent mechanism [22]. Remarkably, *S*. Typhimurium *invA* mutant was significantly impaired in its ability to modulate glucose intake (**S2E Fig**) and ECAR (**Fig 2G**) but its entry into BMDMs was not impaired (**S2F Fig**). On the other hand, *S*. Typhimurium mutant defective for SPI-2-encoded transcriptional regulator *ssrB* was not impaired in its ability to regulate these parameters **(Figs 2G and S2E)**. Furthermore, the *invA* mutant *S*. Typhimurium was also unable to regulate the levels of Glut1 and glycolytic enzymes HK-2 and Enolase upon infection in macrophages (**Fig 2H**). Overall, our analysis suggest that *S*. Typhimurium infection modulated glycolysis is virulence dependent.

Macrophages depend on glycolysis for the clearance of intracellular bacteria

Since we found that *S*. Typhimurium downregulates glycolysis during the later phase of infection in BMDMs, we sought to determine the significance of glycolysis in the macrophage

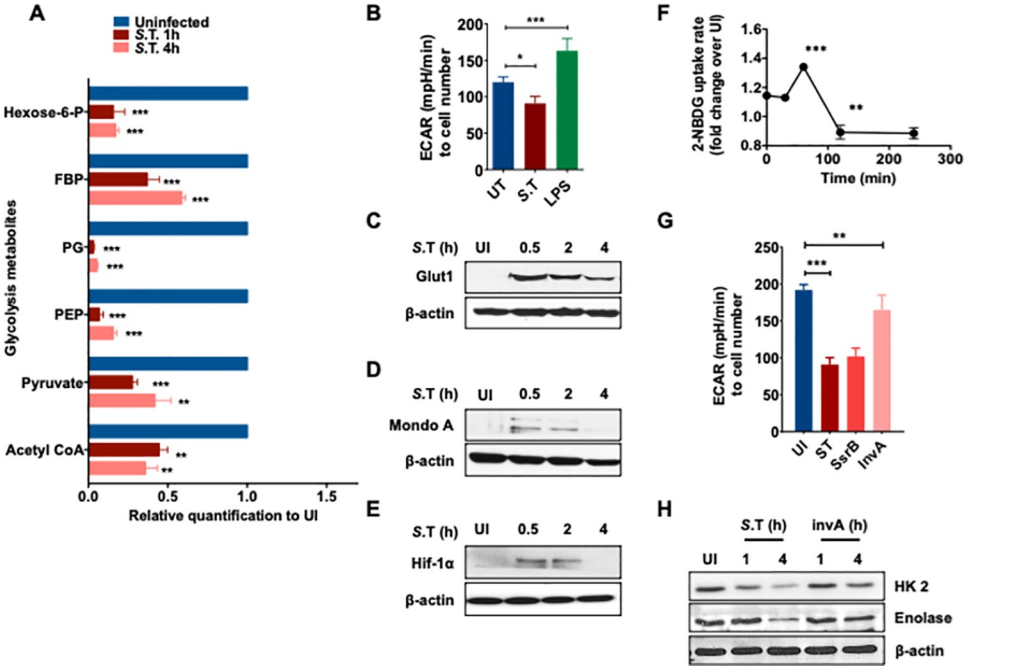

Fig 2. Virulence dependent inhibition of glycolysis in *S*. Typhimurium infected macrophages. (A) Abundance of glycolytic metabolites in S. Typhimurium-infected BMDMs after 1 h and 4 h p.i relative to uninfected (UI) BMDMs (n = 6). **(B)** Extracellular Acidification Rate (ECAR) in BMDMs upon S.T infection or LPS treatment. Data is normalized to cell number (n = 3). **(C)** Western blot analysis of Glut1 **(D)** MondoA **(E)** HIF-1alpha expression at indicated time points upon S. Typhimurium-infected BMDMs compared to uninfected controls. β-actin was used as a loading control. The image shown is representative of 4 independent experiments. **(F)** Kinetics of glucose-intake (shown as 2-NBDG MFI) in S. Typhimurium-infected BMDMs relative to uninfected (UI) BMDMs analyzed by flow cytometry (n = 3). **(G)** Extracellular Acidification Rate (ECAR) in BMDMs infected upon WT, ssrB, and invA mutant *S*. Typhimurium infection. Data is normalized to cell number (n = 6). **(H)** Immunoblot analysis of the protein levels of HexoKinase-2 (HK2, Enolase, and β-actin upon WT and InvA mutant *S*. Typhimurium infection.

https://doi.org/10.1371/journal.ppat.1009943.g002

defense against *S*. Typhimurium. As the predominant function of macrophages is to eliminate invading pathogens, we studied the ability of BMDMs to degrade *S*. Typhimurium following a pre-treatment with the metabolically inactive glucose analogue 2-Deoxyglucose (2-DG) that inhibits glycolysis. Importantly, we found increased number of bacteria in macrophages when glycolysis was inhibited with 2-DG (Fig 3A). Similarly, inhibition of glucose uptake by Glut1 inhibitor Fasentin (S3A Fig) and glucose deprivation using glucose free medium (GFM) (S3B Fig) also increased the number of intracellular bacteria after 24h of infection. However, increasing the concentration of pyruvate in 2-DG-treated and untreated macrophages to fuel mitochondrial metabolism did not rescue the capacity of macrophages to eliminate *S*. Typhimurium (S3C Fig), rather increased the bacterial burden in macrophages, although ATP levels were significantly increased (S3D Fig). This suggests that reduced bacterial clearance upon inhibition of glycolysis is not due to impaired fueling of the mitochondria. Furthermore, we also analyzed the clearance of *S*. Typhimurium by macrophages pre-treated with oligomycin that inhibits mitochondrial ATP production (S3E Fig). Similarly, oligomycin-treated macrophages did not show any impairment in the elimination of *S*. Typhimurium (S3F Fig), suggesting that glycolysis regulates bacterial clearance in mitochondrial ATP-independent manner.

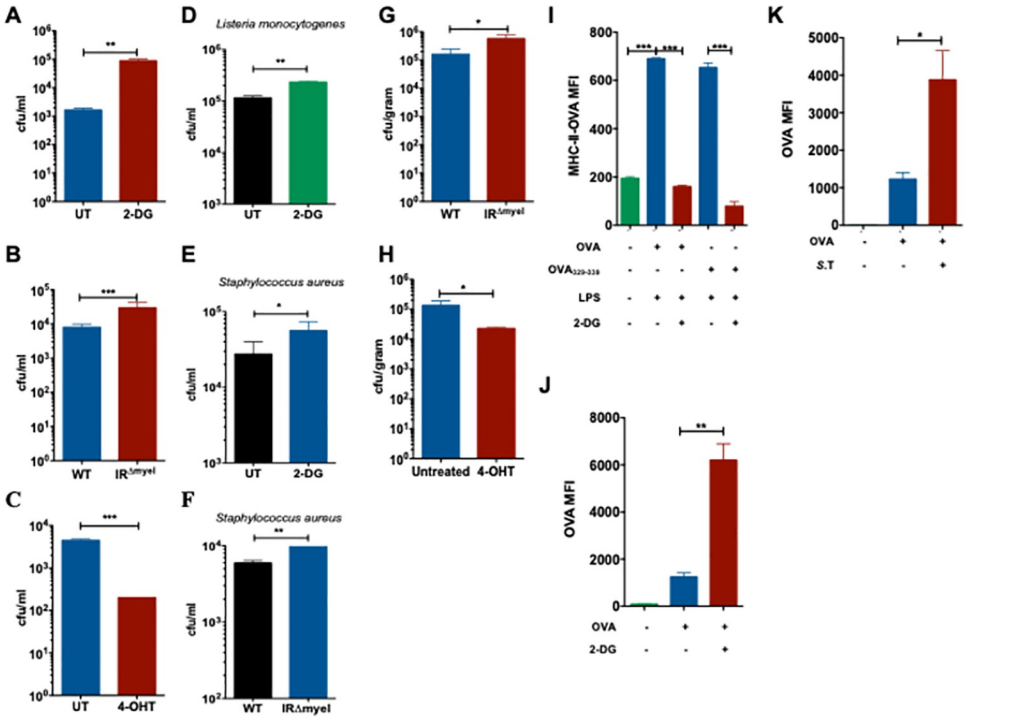

Fig 3. Macrophage depend on glycolysis for the clearance of intracellular bacteria. (A) Bacterial burden expressed as colony forming units (CFU) after 24h of S. Typhimurium infection in 2-DG-treated WT BMDMs compared to untreated (UT) controls (n = 5). **(B)** Intracellular S. Typhimurium load in WT and IR$^{\Delta myel}$ BMDMs after 24h of infection (n = 3). **(C)** S. Typhimurium in 4-OHT-treated WT BMDMs compared to untreated (UT) controls after 24h of infection (n = 3). **(D)** L. monocytogenes **(E)** S. aureus burden in 2-DG-treated WT BMDMs compared to untreated (UT) controls (n = 3). **(F)** S. aureus burden in WT and IR$^{\Delta myel}$ BMDMs (n = 3) 24h post-infection. **(G)** Bacterial load in livers of WT and IR$^{\Delta myel}$ mice after 3 days post *S*. Typhimurium infection or **(H)** 4-OHT-treated mice. Data represent 2 experiments with 5 mice each. Data are shown as mean ± S.E.M. and statistical significance calculated using student t-test and represented as * = p<0.05; ** = p<0.01; *** = p<0.001. **(I)** MFI of OVA323-339-MHC II complexes on the surface of WT BMDMs pre-treated with 2-DG and LPS (n = 3). **(J)** MFI of unprocessed Alexa647-labelled OVA in phagosomes isolated from 2-DG-treated BMDMs analyzed by flow cytometry (n = 3). All samples were pre-stimulated with LPS. **(K)** MFI of unprocessed Alexa647-labelled OVA in bead containing phagosomes isolated from S. Typhimurium-infected BMDMs analyzed by flow cytometry (n = 3).

https://doi.org/10.1371/journal.ppat.1009943.g003

It is well known that insulin signaling modulates glycolysis by regulating the cellular intake of glucose and it has also been shown that myeloid-specific insulin receptor (IR) deficiency alters inflammation [23]. We further show that glucose uptake (S3G Fig) was reduced in $IR^{\Delta myel}$ BMDMs compared to that of the $IR^{fl/fl}$ (WT) BMDMs and also observed a reduction in Glut1 (S3H Fig). Therefore, we next examined whether IR deficiency affects cell-autonomous defense against *S*. Typhimurium in macrophages. IR-deficient macrophages had increased bacterial burden upon infection with *S*. Typhimurium (Fig 3B). However, treatment of macrophages with recombinant insulin did not enhance the elimination of *S*. Typhimurium (S3I Fig). This is not surprising as our data show that insulin receptor and the downstream signaling are down regulated upon *S*. Typhimurium infection **(Figs 1D, S1E and S1F)**. Strikingly, when glucose uptake (S4A Fig) and ECAR (S4B Fig) were enhanced upon treatment with the glycolysis activator 4-hydroxytamoxifen (4-OHT) as reported before [24, 25] and bacterial burden was significantly decreased (Fig 3C). Importantly, inhibition of glycolysis using 2-DG prevented enhanced bacterial clearance triggered by the treatment of 4-OHT (S4C **Fig**), confirming that 4-OHT-mediated enhanced bacterial elimination is glycolysis-dependent. Neither 2-DG nor 4-OHT directly impacted the growth of the bacteria **(**S4D Fig**)**. Moreover, we found that the requirement of glycolysis for the clearance of intracellular bacteria is not specific for *S*. Typhimurium. Pathogens such as *Listeria monocytogenes (L. monocytogenes)* (Fig 3D) *and Staphylococcus aureus (S. aureus)* (Fig 3E) also survived better in 2-DG-treated macrophages. Similarly, IR-deficient macrophages also showed reduced ability to eliminate *S. aureus* (Fig 3F). Together, our results suggest that glycolysis plays a significant role in the elimination of intracellular bacteria.

Consistent with the increase in bacterial burden, secretion of pro-inflammatory cytokines IL-6 and TNF-α was also increased when 2-DG-treated macrophages were infected with *S*. Typhimurium **(**S4E Fig**)**, *L. monocytogenes* (S4F Fig) or *S. aureus* (S4G Fig). Similar reduction in proinflammatory cytokines was observed when GFM-treated (S4H Fig) or $IR^{\Delta myel}$ macrophages were infected with *S*. Typhimurium (S4I Fig). In line with these findings, *S*. Typhimurium-induced IL-6 and TNF-α levels were decreased when glycolysis was induced with 4-OHT (S4J Fig). Increased cytokine secretion upon 2-DG treatment also correlated with the enhanced activation of NF-κB and p38 MAPK (S4K Fig). Next, we sought to investigate the involvement of glycolysis to control *S*. Typhimurium infection *in vivo*. Consistent with the *in vitro* results obtained in BMDMs, $IR^{\Delta myel}$ mice had increased bacterial burden in the liver after 3 days of *S*. Typhimurium infection compared to WT controls (Fig 3G). In contrast, 4-OHT-treated WT mice had significantly reduced *S*. Typhimurium in the liver (Fig 3H). Taken together, these results clearly suggest that increased glycolysis is beneficial for the clearance of bacteria *in vivo*.

Having found that glycolysis is required for the elimination of bacteria, we investigated whether the antigen processing and presentation could also be affected in macrophages when glycolysis is inhibited. To test this, we incubated 2-DG-treated and LPS-stimulated BMDMs with Ovalbumin (OVA) and analyzed the surface expression of the OVA peptide $OVA_{323\text{-}339}$ bound to the MHC class II complex using OVA-specific antibodies by flow cytometry. We found that 2-DG-treatment drastically decreased the levels of $OVA_{323\text{-}339}$-MHC II complexes on the surface of macrophages (Fig 3I). To gain better insight into the effect of glycolysis on antigen processing inside the phagosome, we incubated 2-DG-treated macrophages with beads coated with OVA conjugated to Alexa Fluor 647 dye. Analysis of the fluorescence intensity of the isolated phagosomes showed increased retention of Alexa647-OVA in 2-DG-treated macrophages suggesting reduced processing of the antigen (Fig 3J). Similarly, inhibition of glycolysis by *S*. Typhimurium infection also resulted in decreased processing of Alexa647-OVA as seen by the increased mean fluorescence intensity (MFI) in isolated

Alexa647-OVA-coated-bead-containing phagosomes (Fig 3K). The decrease in processing of Alexa647-OVA caused by *S*. Typhimurium infection was partially rescued by treatment with 4-OHT (S4L Fig). Taken together, these data demonstrate that glycolysis is required for efficient antigen processing and antigen presentation.

Glycolysis is crucial for phagosome maturation upon infection in macrophages

Macrophages engulf invading pathogens into phagosomes, which later fuse with lysosomes to degrade the pathogens. Increase in bacterial burden upon inhibition of glycolysis hinted that glycolysis could possibly regulate phagosomal functions in macrophages. To understand the role of glycolysis in phagosome maturation, we performed a series of flow cytometric assays to analyze the β-galactosidase and proteolytic activities in phagolysosomes containing inert beads in macrophages. To this end, beads either coated with C_{12}FDG (a substrate for β-galactosidase) or with DQ-BSA (a substrate for proteases) were incubated with the macrophages. These substrates fluoresce when they react with their corresponding enzymes. Notably, 2-DG treatment prior to phagocytosis of beads showed markedly reduced β-galactosidase (Fig 4A) and proteolytic activities (Fig 4B) in fluorescent bead (APC)-containing phagosomes. A similar decrease in the activities of β-galactosidase (Fig 4C) and proteases (Fig 4D) was also observed in

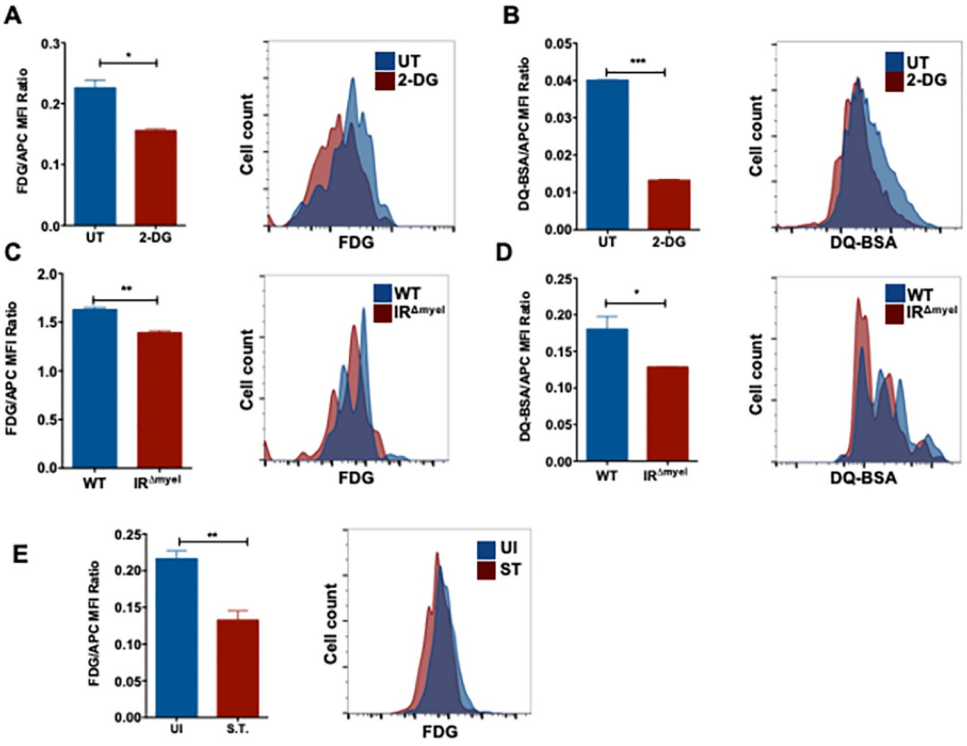

Fig 4. Glycolysis is crucial for phagosome maturation upon infection in macrophages. (A) Flow cytometry analysis of 2-DG pre-treated macrophages pulsed with C12FDG-coated fluorescent (APC) beads (n = 3) and **(B)** DQ-BSA-coated fluorescent (APC) beads (n = 3). Bar graphs represent mean fluorescence intensities (MFI) of C12FDG and DQ-BSA normalized to MFI of red fluorescence (APC). MFI of **(C)** C12FDG and **(D)** DQ-BSA in WT and IRΔmyel BMDMs normalized to MFI of red fluorescence (n = 3). **(E)** Flow cytometric analysis of BMDMs infected with C12FDG and Alexa594-coated *S*. Typhimurium for 2h in WT BMDMs. Bar graphs represent the mean MFI of C12FDG normalized to MFI of red fluorescence. Data are representative of at least three independent experiments with 3 replicates each. Data are shown as mean ± S.E.M. and statistical significance calculated using student t-test is represented as * = $p<0.05$; ** = $p<0.01$; *** = $p<0.001$.

https://doi.org/10.1371/journal.ppat.1009943.g004

IR-deficient macrophages when compared to WT controls. However, no significant differences in the phagocytosis of fluorescent beads were observed in 2-DG-treated or IR-deficient macrophages compared to untreated or WT controls, respectively (S5A and S5B Fig). To test if *S*. Typhimurium mediated downregulation of glycolysis mimicked the effect of 2-DG, macrophages were infected for 2h to ensure that *S*. Typhimurium downregulated glycolysis. Cells were then allowed to phagocytose C_{12}FDG-coated beads, which were chased into phagolysosomes and the activity of β-galactosidase was analyzed by flow cytometry. Interestingly, β-galactosidase activity on C_{12}FDG-labelled beads phagocytosed after 2h of *S*. Typhimurium infection was reduced compared to the activity on C_{12}FDG-labelled-beads phagocytosed by uninfected cells (Fig 4E). Furthermore, we found increased fluorescence signal from C_{12}FDG-labelled beads that were phagocytosed after 30 min of *S*. Typhimurium infection, corresponding to the time when *S*. Typhimurium transiently increased glycolysis (S5C Fig). These results suggest that glycolysis is required for the efficient functioning of phagolysosomes and *S*. Typhimurium prevents this during the later phase of infection by downregulating glycolysis.

Glycolysis critically regulates the acidification of phagosome and the assembly of v-ATPase complex

The activity of lysosomal enzymes and the maturation of the phagosomes to phagolysosomes are highly dependent on the acidification of the vesicle [26]. Since inhibition of glycolysis impaired the activity of lysosomal enzymes in macrophages, we investigated if there is a defect in the acidification of the phagosomal lumen. Acidification of the phagosomes was studied using *E. coli* bioparticles labelled with pHrodo, a pH sensitive dye, which increases fluorescence intensity upon acidification. Notably, phagosome acidification was significantly reduced in fluorescent bioparticle (Alexa647)-containing phagosomes in macrophages pre-treated with 2-DG (Fig 5A) or treated with GFM (S6A Fig) when compared to untreated controls. Consistently, acidification was also limited in bioparticle-containing phagosomes of $IR^{\Delta myel}$ macrophages compared to WT controls (Fig 5B). Furthermore, *S*. Typhimurium-mediated inhibition of glycolysis also impaired acidification of bioparticle-containing phagosomes (Fig 5C), but the acidification was increased upon infection with *invA* mutant (S6B Fig). Also, acidification of *S*. Typhimurium-containing phagosomes increased upon treatment with 4-OHT (S6B Fig). Remarkably, the observed decrease in acidification of bead containing phagolysosomes in *S*. Typhimurium-infected macrophages was rescued when treated with 4-OHT (Fig 5D), suggesting that *S*. Typhimurium prevents phagolysosome acidification by impairing glycolysis.

Acidification of phagosomes is mediated by a multimeric protein complex known as vacuolar-ATPase (v-ATPase), which is composed of 14 subunits organized in two main catalytic macro domains: V_0 and V_1 [27]. While V_0 is permanently bound to the membrane of phagosomes, V_1 is located in the cytosol and is actively recruited onto the phagosome to interact with V_0 and thus activate the proton pump [28]. To test whether inhibition of glycolysis could have an effect on the assembly of the v-ATPase complex in macrophages, isolated bead containing-phagosomes from 2-DG-treated BMDMs and $IR^{\Delta myel}$ BMDMs were analyzed for the expression of subunit-*a* and subunit-B which are part of the V_0 and the V_1 macro domains, respectively. V_0 subunit-*a* was detected in comparable amounts in bead containing-phagosomes isolated from 2-DG-treated for 2h and untreated controls (Fig 5E). Similarly, abundance of V_0 subunit-*a* was comparable in phagosomes isolated from $IR^{\Delta myel}$ macrophages and the WT controls (Fig 5G). However, the expression of the V_1 subunit-B was reduced in the phagosomes isolated from 2-DG-treated macrophages (Fig 5E and 5F). Similarly, we found reduced levels of the V_1 subunit-B in bead containing-phagosomes isolated from $IR^{\Delta myel}$

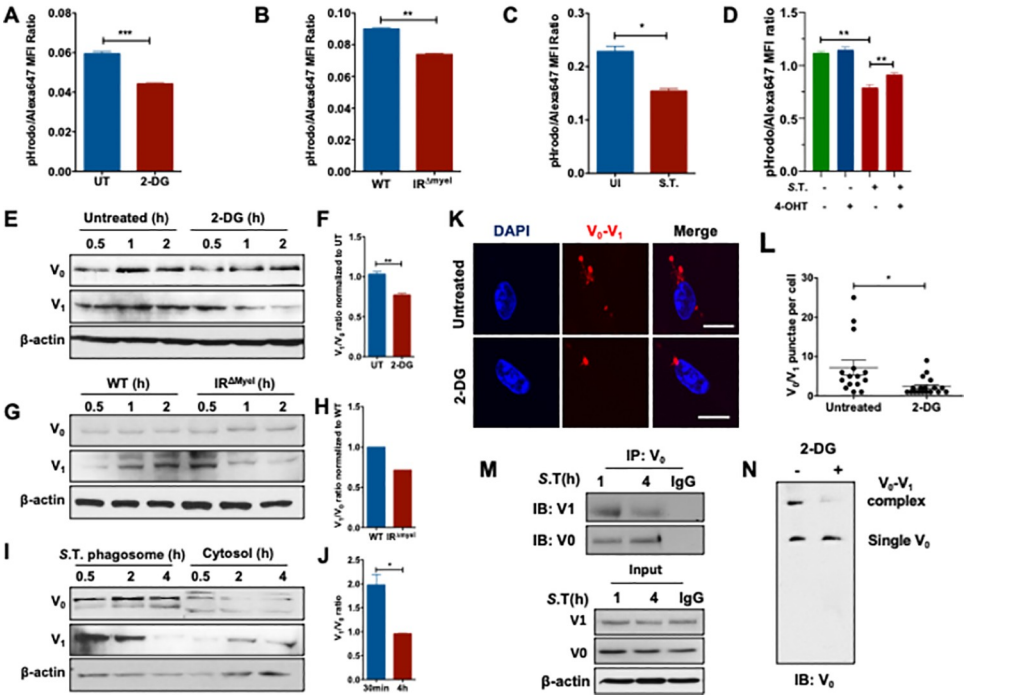

Fig 5. Glycolysis critically regulates the acidification of phagosomes and assembly of v-ATPase complex. (A) MFI of pH-sensitive pHrodo-E. coli particles in BMDMs untreated (UT) or pre-treated with 2-DG, normalized to Alexa647 MFI (n = 3). **(B)** MFI of pHrodo-E. coli particles in WT and $IR^{\Delta myel}$ BMDMs normalized to Alexa647 MFI (n = 3). **(C)** MFI of pHrodo-E. coli particles in S. Typhimurium-infected WT BMDMs (2h p.i.) normalized to Alexa647 MFI (n = 3). **(D)** MFI of pHrodo-E. coli particles in 4-OHT-treated BMDMs infected with S. Typhimurium for 2h normalized to Alexa647 MFI (n = 3). **(E-F)** Expression of v-ATPase subunits (V0, V1) in isolated bead-containing phagosomes from untreated and 2-DG-treated BMDMs. The image shown is representative of 3 individual experiments. Immunoblot band intensities were quantified using ImageJ and the V1/ V0 ratio was determined and plotted (n = 3). **(G-H)** Expression of v-ATPase subunits (V0, V1) in isolated bead phagosomes from WT and $IR^{\Delta myel}$ BMDMs. Western blot was quantified and V1/V0 ratios are shown. Expression of v-ATPase subunits (V0, V1) in isolated S. Typhimurium phagosomes and cytoplasm. V1/V0 ratios were quantified and plotted. **(I-J)** V0 subunit A was immunoblotted from isolated *S.* Typhimurium phagosomes and probed for V1 subunit B. **(K-L)** Proximity Ligation Assay (PLA) analysis of V0-aldolase A interaction in 2-DG treated BMDMs. The image shown is representative of 3 individual experiments. **(M)** Immunoprecipitation of V0 subunit from *S.* Typhimurium infected phagosomes at indicated times probed for V1, V0 and actin. Rabbit IgG was used as a control for immunoprecipitation. **(N)** Phagosomes isolated from 2DG-treated and untreated macrophages were subjected to Native-PAGE and immunoblotted for v-ATPase subunits V0 and V1.

https://doi.org/10.1371/journal.ppat.1009943.g005

macrophages (Fig 5G and 5H) and from fasentin-treated macrophages when compared to WT controls (S6C Fig). Notably, we did not observe differential amounts of V_0 and V_1 subunits in the total cell lysates of 2-DG-treated macrophages compared to controls (S6D Fig) or in fasentin-treated cells compared to untreated controls (S6E Fig). These findings suggest that impaired glycolysis prevents the assembly of the v-ATPase complex rather than the expression itself. V_1 recruitment on to phagosomes containing *S.* Typhimurium was also reduced, while V_0 levels did not vary significantly between different time points (Fig 5I). The decline in V_1 on phagosomes harboring *S.* Typhimurium corresponded with the time when glycolysis was inhibited (Fig 2A–2E). Similarly, Proximity Ligation Assay (PLA) also showed reduced interaction of V_0 and V_1 in 2-DG-treated macrophages (Fig 5K and 5L). The decreased interaction between V_0 and V_1 upon *S.* Typhimurium infection was also confirmed by PLA (S6F and S6G Fig). We also immunoprecipitated (IP) V_0 from isolated *S.* Typhimurium-containing phagosomes and observed the complex formation of V_0 and V_1 however, V_1 binding to V_0 was

reduced in *S*. Typhimurium-phagosomes isolated after 6h (Fig 5M). Similarly, V1 binding to V0 was reduced in bead containing phagosomes isolated from GFM-treated macrophages (S7A Fig). To further investigate the effect of the inhibition of glycolysis on v-ATPase complex formation, we conducted Native SDS-PAGE using isolated bead- containing phagosomes from macrophages treated with 2-DG or GFM. 2-DG (Fig 5N) or GFM (S7B Fig) treatment resulted in a significant decrease in the formation of v-ATPase complex. Taken together, these results strongly suggest that glycolysis plays a critical role in the assembly of v-ATPase.

Aldolase A critically regulates the assembly of v-ATPase and phagosome acidification

Glycolytic enzymes aldolase A and phosphofructokinase-1 (PFK1) have been shown to interact with different subunits of the v-ATPase in yeast, likely acting as scaffold proteins and are required for the acidification of endosomes [29, 30]. Confocal microscopy confirmed that aldolase A colocalized with inert *E. coli* bioparticles-containing phagosomes when glucose was abundant (Fig 6A). However, co-localization of aldolase A with *E. coli* particles-containing

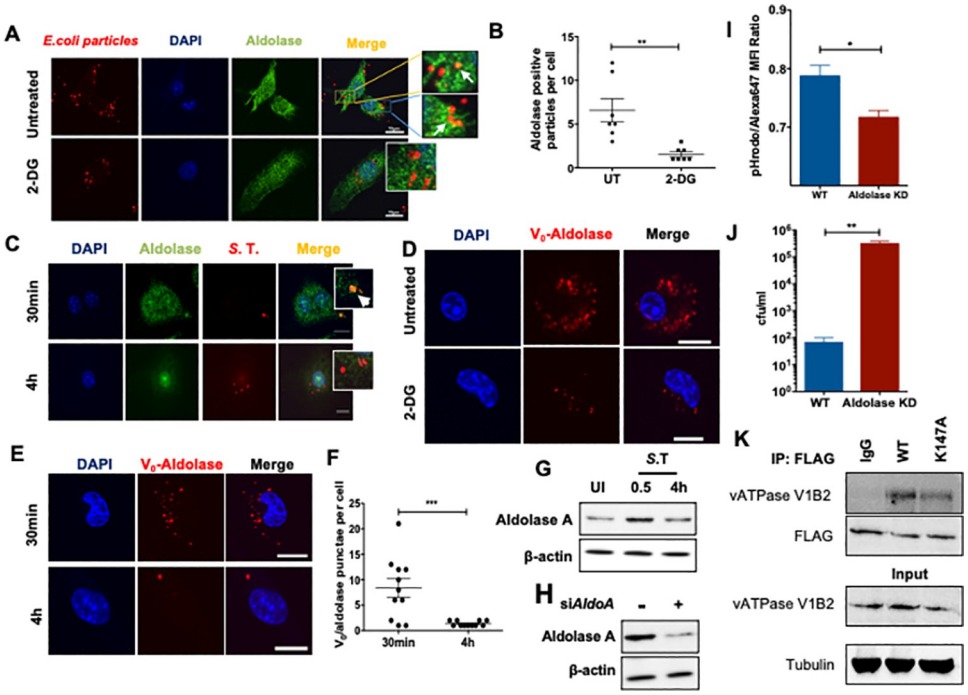

Fig 6. Aldolase A critically regulates the assembly of v-ATPase and phagosome acidification. **(A)** Confocal microscopy of 2-DG-treated BMDMs pulsed with E. coli inert fluorescent particles immune stained for aldolase A (green) (scale bars indicate 10μm). The image shown is representative of 3 individual experiments. **(B)** Quantification of aldolase A co-localization with E. coli in 2-DG-treated BMDMs (n = 7). **(C)** Confocal microscopy of S. Typhimurium-infected (S.T., red) BMDMs immune stained for aldolase A (green). The image shown is representative of 3 individual experiments. **(D)** PLA analysis of V0-aldolase A interaction in 2-DG treated BMDMs. The image shown is representative of 3 individual experiments. **(E)** PLA analysis of V0-aldolase A interaction in S. Typhimurium-infected BMDMs at indicated times. The image shown is representative of 3 individual experiments. **(F)** Quantification of V0 and aldolase A interaction in S. Typhimurium-infected BMDMs (n = 10). **(G)** Western blot analysis of Aldolase A expression in BMDMs infected with S. Typhimurium at indicated time points. (**H**) Knockdown of Aldolase A in BMDMs using control siRNA and Aldolase A-specific siRNA. The expression of Aldolase A was analyzed 48h post-transfection. **(I)** MFI of pHrodo-E. coli particles in transient aldolase A KD BMDMs normalized to Alexa647 MFI analyzed by flow cytometry (n = 3). **(J)** Quantification of S. Typhimurium CFU in aldolase A KD macrophages 24h post-infection compared to WT controls (n = 3). **(K)** BMDMs ectopically expressing FLAG-tagged WT or catalytic mutant aldolase A was immunoprecipitated and probed with indicated antibodies.

https://doi.org/10.1371/journal.ppat.1009943.g006

phagosomes was significantly reduced upon glycolysis-inhibition with 2-DG (Fig 6A and 6B). Aldolase A colocalized with *S*. Typhimurium-containing phagosomes as early as 30 min post infection, but the amount of *S*. Typhimurium-phagosomes positive for aldolase A was reduced at 4h post infection (Fig 6C). Reduced presence of aldolase A on isolated *S*. Typhimurium phagosomes was confirmed by Western blotting (S8A Fig). PLA analysis revealed interaction between V_0 and Aldolase A in untreated macrophages. However, the number of red puncta (indicating interaction between V_0 and Aldolase A) was significantly reduced upon treatment with 2-DG (Fig 6D). V_0 and Aldolase A interaction was also observed in *S*. Typhimurium-infected macrophages but the frequency of puncta per cell reduced after 4h of infection compared to 30 min (Fig 6E and 6F). Total levels of aldolase A also showed a modest increase in macrophages upon *S*. Typhimurium infection (Fig 6G). Since we observed that the reduction in the recruitment of aldolase A on to bead or *S*. Typhimurium-containing phagolysosomes correlated with the decrease in phagosome acidification, we sought to determine if aldolase A played a role in the regulation of phagolysosome acidification. Short interfering RNA (siRNA)-mediated knockdown (KD) of Aldolase A in BMDMs (Fig 6H) significantly reduced phagosomal acidification as indicated by reduced pHrodo fluorescence in aldolase A-depleted BMDMs (Fig 6I). As a direct consequence of reduced phagosome acidification, Aldolase A depletion also significantly inhibited phagosomal processing as evident from increased number of intracellular *S*. Typhimurium after 24h of infection (Fig 6J). We next wished to understand whether the interaction of Aldolase A with v-ATPase complex is dependent on its enzymatic activity. K147 residue in aldolase A has been shown to be critical for substrate binding and enzymatic activity [31, 32]. We generated Flag-tagged, catalytically inactive mutant of aldolase A (K147A) and investigated its interaction with V-ATPase subunit V1B2 in 293T cells. We observed that Aldolase A and V1B2 interaction was independent of the catalytic activity of aldolase A (Fig 5K). Taken together, our data signifies the roles of glycolysis and glycolytic enzyme aldolase A in the assembly of v-ATPase, vacuolar acidification and clearance of intracellular bacteria (Fig 7).

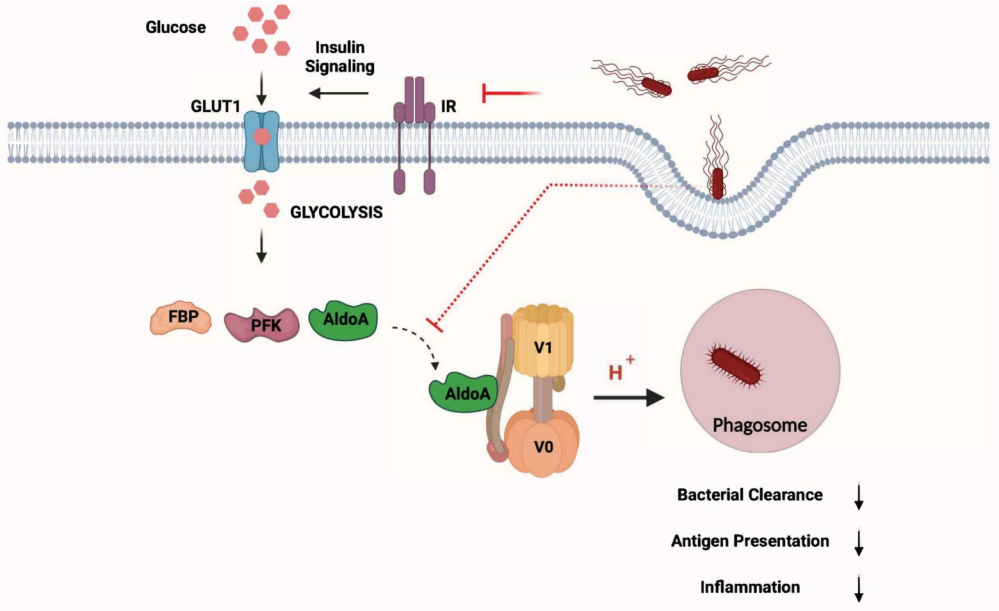

Fig 7. Schematic representation of S. Typhimurium-mediated evasion of phagosome degradation in macrophages by preventing glycolysis-regulated assembly of the v-ATPase.

https://doi.org/10.1371/journal.ppat.1009943.g007

Discussion

Upon pro-inflammatory stimuli, macrophages undergo metabolic reprogramming as part of an innate immune response. In this study, we deciphered that *S*. Typhimurium down regulates glycolysis, which is critical for phagolysosomal function and antigen-presentation in macrophages. We further demonstrate that glycolysis is required for the assembly of v-ATPase complex on phagosomes and acidification of phagosomes, which is coordinated by aldolase A.

An orchestrated and effective immune response requires high levels of ATP and biomolecules. However, sites of infection are often poor in oxygen and nutrients. It has become evident that, macrophages and dendritic cells undergo a metabolic shift similar to the Warburg-effect observed in cancer cells when pattern recognition receptors are activated to meet the high-energy demand [33]. Similarly, intracellular pathogens must adapt to survive in the hostile intracellular milieu, which requires altering the metabolic environment to its advantage. In this regard, it is interesting to note that pathogenicity of *Mycobacterium tuberculosis* has been linked to its ability to modulate cellular metabolism [34]. *S*. Typhimurium is a facultative intracellular pathogen that is known to alter mitochondrial metabolism in host cells and reduce ATP production [14, 35–37]. However, the specific regulation of host metabolic pathways and its interplay with innate immune mechanisms upon *S*. Typhimurium infection remain unknown. Our metabolomics and transcriptomics analysis converged in revealing that the central-carbon-metabolism pathways contributing to ATP generation in macrophages, namely glycolysis, the TCA cycle and the mitochondrial electron transport chain, were markedly down regulated upon infection with *S*. Typhimurium. Our results are in agreement with previous microarray analysis conducted on colon mucosa and liver of *S*. Typhimurium-infected mice, where a decline in OXPHOS and carbohydrate metabolism together with decreased levels of hormones regulating the metabolic pathways have been reported [38, 39]. Furthermore, down regulation of these metabolic pathways is consistent with the previously reported necrotic cell death and ATP depletion induced by *S*. Typhimurium [2]. Additionally, *S*. Typhimurium-mediated down regulation of glycolytic metabolites could be a direct effect of bacterial metabolism, since *S*. Typhimurium in macrophages has been shown to rely on glycolysis for its replication, reducing the availability of glucose in the host cytosol [13]. Furthermore, we had also shown that *S*. Typhimurium downregulates AMPK which upon activation can increase glycolysis [14]. Taken together, our results highlight glycolysis as a key target of *S*. Typhimurium during its interplay with host cells. On the contrary, a recent report shows that glycolysis is increased in *S*. Typhimurium strain ATCC 14028s-infected sodium periodate activated peritoneal macrophages [40] and *S*. Typhimurium strain SL1344 in RAW macrophages [41]. It is important to note that disruption of glycolysis is linked to inflammasome-mediated cell death [42]. However, Jiang et al [40] were able to see an increase in glycolysis up to 20h using strain ATCC 14028s and Ding et al [41] have shown apoptosis in RAW macrophages using strain SL1344. Therefore, the discrepancies can be attributed to the macrophage model and the strain of bacteria used.

Emerging evidence suggests that Warburg effect-like metabolic shift observed in macrophages fuel inflammatory responses when exposed to TLR agonists [43]. The metabolic shift towards glycolytic flux fuels both the TCA cycle and the pentose phosphate pathway (PPP) thus providing a double impact on the innate immune defense mechanisms. On the one hand, increased production of NADPH by the PPP results in ROS-mediated inflammation as a consequence of the transfer of electrons from NADPH to NADPH-oxidase [44]. Metabolites such as succinate derived from TCA cycle have also been shown to induce IL-1β in a HIF-1α-dependent manner in macrophages stimulated with LPS [11]. In contrast, our data indicate that *S*. Typhimurium-induced inflammation is independent of these metabolic mechanisms

since levels of ribose-5-phosphate (PPP), and succinate (TCA cycle) declined. Moreover, inhibition of glycolysis further enhanced inflammatory cytokine secretion in *S*. Typhimurium-infected macrophages. Our data corroborates with the report that *S*. Typhimurium disrupts glycolysis to induce inflammasome-mediated inflammation [42]. Therefore, we propose that *S*. Typhimurium inhibits glycolysis to evade phagosomal clearance leading to the activation of canonical inflammatory pathways.

A predominant function of macrophages is to phagocytose invading pathogens and eliminate them in phagolysosomes. Previous reports have shown that *S*. Typhimurium prevents fusion of lysosomes with bacteria-containing phagosomes [45]. Contradictorily, several other studies have shown that *S*. Typhimurium-containing vacuoles (SCVs) are accessible to lysosomal markers and they fuse with lysosomes [46, 47]. This paradox could be clarified by our findings, which show that macrophages initially upregulate glycolytic machinery to enhance acidification of the phagosomes and acquire late endosomal properties. However, *S*. Typhimurium uses the phagosomal acidic environment to express its SPI-2-encoded virulence factors [48] and inhibit phagosome maturation. This phenomenon correlates with our observation; rapid increase in Glut1 expression, glucose import and acidification of phagosomes followed by a marked reduction at the later phase of infection. Interestingly, we also observed that the reduction in glucose import and acidification of phagosomes is virulence associated and is partially SPI-I-dependent as the *S*. Typhimurium mutant *invA* did not abrogate glycolysis as that of the WT bacteria (**Fig 2G and 2H**). However, other SPI-I effector proteins could be involved in modulating glycolysis as it has been recently demonstrated that the SPI-1 effector SopE2 represses serine synthesis down stream of glycolysis [40].

Our findings clearly demonstrate that reduced glycolysis due to deficient insulin signaling or feeding cells with 2-DG leads to increased bacterial replication *in vitro* and *in vivo*. 4-OHT has been known to enhance glucose uptake and glycolytic flux by activating AKT [24] and AMPK [25] in cancer cells. Accordingly, up regulation of glycolysis using 4-OHT starkly reduced bacterial burden in BMDMs and *in vivo*. These results indicate that metabolism is intricately linked to phagosomal functions in macrophages. Our investigations using inert biological particles and beads coated with substrates for various lysosomal enzymes reveal a general cellular mechanism that glycolysis regulates the activity of lysosomal enzymes. *S*. Typhimurium-mediated inhibition of glycolysis also reduced the processing and presentation of OVA peptides on MHC molecules. This is consistent with our previous report that *S*. Typhimurium-infected antigen presenting cells lack antigen presentation ability [49]. Interestingly, both the processing of antigens and the activation of MHC II (cleavage of the invariant chain) are pH-dependent [50].

Acidification of the phagosomes is a prerequisite for the degradative function, because lysosomal enzymes require acidic pH for their optimal activity. Acidification is also required for the interaction with endocytic vesicles and the maturation of phagosomes themselves [51]. Metabolic intermediates such as ROS catalyzed by NADPH-oxidase and generated in mitochondria juxtaposed to pathogen containing phagosomes [52] and NADH-dependent NO production by iNOS [53] have been shown to facilitate the bactericidal activity of phagolysosomes. Production of these metabolic intermediates also requires protons generated by v-ATPase complex. Acidification of phagosomes is regulated by the multimeric complex v-ATPase and is critical for the maturation of phagosomes, fusion of lysosome with phagosomes and the activity of lysosomal enzymes [54, 55]. Since we observed defects in phagosome maturation in glycolysis-deficient macrophages, we reasoned that glycolysis could be involved in the acidification of phagosomes. As expected, under conditions of reduced glycolytic flux, acidification of phagosomes containing inert biological particles was significantly reduced, which is a result of defective assembly of V_0 and V_1 on phagosomes. Our study thus suggests

that *S*. Typhimurium mediated down regulation of glycolysis prevents acidification of the pathogen-containing phagosomes by hampering the assembly of V_0 and V_1 on the phagosomes. This is consistent with a previous report demonstrating that high glucose availability facilitates the assembly of v-ATPase thus enabling increased entry of influenza virus [56]. However, the mechanism remains poorly characterized.

We found that glycolytic enzymes were downregulated when glucose intake was reduced by *S*. Typhimurium infection, indicating that the import of glucose could be an additional mechanism regulating the expression of glycolytic enzymes. Consistently, we observed a decrease in MondoA over time, a glucose-induced transcription factor responsible for the transcriptional regulation of enzymes involved in carbohydrate catabolism, including glycolysis and PPP [57]. Glycolytic enzymes are also known to perform multifaceted non-glycolytic functions such as transcriptional regulation [58], cell motility and regulation of apoptosis [59]. Glycolytic enzymes such as aldolase and PFK have been directly implicated in the assembly of v-ATPase [29, 30]. Future studies on the specific roles of different glycolytic enzymes in the regulation of phagosomes will be valuable in understanding the process of phagosome maturation and will expand its role in linking innate and adaptive immunity.

Taken together, our findings convincingly demonstrate that glycolysis critically regulates the phagolysosomal activity of macrophages, which is evaded by *S*. Typhimurium. Conceivably, in pathological conditions such as diabetes wherein cells are insensitive to insulin, patients become increasingly susceptible to infections because macrophages will be inefficient in eliminating pathogens as a result of reduced glycolysis. Furthermore, the significance of glycolysis in antigen processing and presentation could be applied in designing adjuvants for vaccines. Finally, increase in antimicrobial properties of macrophages upon 4-OHT treatment suggests an alternate approach to control drug-resistant pathogens.

Experimental procedures

Ethics statement. All animal procedures were in accordance with institutional guidelines on animal welfare and were approved by the North Rhine-Westphalian State Agency for Nature, Environment, and Consumer Protection [Landesamt für Natur, Umwelt and Verbraucherschutz (LANUV) Nordrhein-Westfalen; File no: 84–02.05.40.14.082 and 84–02.04.2015. A443] and the University of Cologne.

Preparation of bacteria. Bacteria from a single colony was inoculated into 5 mL of BHI medium and incubated overnight at 37˚C with constant agitation. Next, 1 mL of bacteria suspension was transferred into 50 mL of BHI and grown until it reached OD_{600} value of 1.0 (stationary phase). The concentration of bacteria was estimated by plating serial dilutions on BHI agar plates. When indicated, *S*. Typhimurium was inactivated for 10 min at 95˚ C.

Cell culture and bacterial infection. Bone marrow was extracted from femur of 8–12 weeks old female wild-type (WT) C57BL/6 mice (Charles River Laboratories) or insulin receptor knockout ($IR^{\Delta myel}$) mice (provided by Jens Brüning, MPI for Metabolism and Ageing, Cologne, Germany). Bone marrow was differentiated into macrophages for 7 days in RPMI medium supplemented with 20% L929 supernatant and 10% fetal bovine serum (FBS). Bone marrow derived macrophages (BMDMs) were infected with *S*. Typhimurium SL1344 or *S. aureus or L. monocytogenes* at a multiplicity of infection (MOI) of 10. After infection, BMDMs were incubated with the bacteria for 10 min at RT and 30 min at 37˚C. This incubation time was sufficient for bacteria to be internalized by macrophages as confirmed by microscopy analysis. Cells were then washed with medium containing 50 μg/ml of gentamicin and incubated in medium with 50 μg/ml of gentamicin. After 2h, the concentration of gentamycin was reduced to 10 μg/ml. BMDMs were treated with 1 mM 2-DG (Life Technologies) dissolved in

medium without glucose for 2h prior to infection, 1 μM 4-hydroxytamoxifen (4-OHT; Sigma) for 1h at 37˚C prior to infection and during the course of infection, oligomycin (Sigma) 2 μg/ml for 30 min prior to infection, pyruvate 1mM for 2h prior to infection or with *S*. Typhimurium LPS (Sigma) 100 ng/ml for the indicated times.

Targeted metabolomics analysis. $1x10^6$ cells per sample were taken for metabolomics analysis. Trypsinized cells were washed twice with PBS buffer and then with deionized water for few seconds. Subsequently, cells were quickly quenched in liquid nitrogen and stored at -80˚C until further analysis. Frozen cell samples were thawed step wise at -20˚C and 4˚C and then metabolites were extracted by adding 20 μl of labeled internal standard mix and 1 ml of cold extraction solvent (90/10 ACN/H2O + 1% FA). Cells were then vortexed for 30 sec, sonicated for 30 sec in three cycles, and incubated on ice for 10 min. After the centrifugation at 14000 rpm for 15 min at 4˚C, 800 μl of supernatants were aspirated into Eppendorf tubes. The collected extracts were dispensed in Ostro 96-well plate (Waters Corporation, Milford, USA) and filtered by applying vacuum at a delta pressure of 300-400mbar for 2.5 min on robot's vacuum station. The clean extract was collected to a 96-well collection plate, placed under Ostro plate. The collection plate was sealed and centrifuged for 15 min, 4000 rpm, 4˚C and placed in auto-sampler of the liquid chromatography system for the injection. Isotopically labeled internal standards were obtained from Cambridge Isotope Laboratory. Inc., USA (S1 Table). Instrument parameters, analytical conditions and data analysis were performed as previously described [60]. Metabolomics data analysis was carried out using a web-based comprehensive metabolomics data processing tool, MetaboAnalyst 3.0 [61]. Log-transformed and auto scaled data i.e., mean-centered and divided by the standard deviation of each variable, was used for various data analysis. t-test for unequal variances (Welch's t-test) was applied by default to every compound.

RNA-sequencing. Total RNA from *S*. Typhimurium-infected BMDMs was extracted 2 h post infection using the Qiagen RNAeasy kit and cDNA was synthesized with SuperScript III (Life Technologies) following the manufacturer's instructions. For Illumina sequencing, libraries were prepared from total RNA with Ribo-Zero treatment according to the manufacturer's instructions. The analysis was carried out using the standardized RNA-Seq workflow on the QuickNGS platform [62]. In brief, reads were aligned to the GRCm38 (mm10) build of the mouse genome using TopHat2 [63] and FPKM values were computed with Cufflinks [64]. The sequence data has been submitted to GEO repository and can be accessed using the accession number GSE84375. Differential gene expression analysis was carried out using DEseq2 [65] on the raw read counts based on release 82 of the Ensembl database. Finally, genes were selected according to a threshold of 2 for the fold change and 0.05 for the p-value.

Analysis of glycolytic metabolites. Metabolites pertaining to glycolysis were analyzed with the assistance of Metabolomic Discoveries, Berlin, Germany. At the indicated time points post-infection, BMDMs were washed with cold 0.9% NaCl and cells were collected in extraction buffer provided by Metabolomic Discoveries. Samples were snap-frozen and sent to Metabolomic Discoveries. Derivatization and analysis of metabolites by a GC-MS 7890A mass spectrometer (Agilent, Santa Clara, USA) were carried out as described [50]. Metabolites were identified in comparison to Metabolomic Discoveries database entries of authentic standards. The LC separation was performed using hydrophilic interaction chromatography with a ZIC-HILIC 3.5μm, 200A column (Merck Sequant, Umeå Sweden), operated by an Agilent 1290 UPLC system (Agilent, Santa Clara, USA). The LC mobile phase was A) 95% acetonitrile; 5% 10 mM ammonium acetate and B) 95% 10mM ammonium acetate; 5% acetonitrile with a gradient from 95% A to 72% A at 7 min, to 5% at 8 min, followed by 3 min wash with 5% A. The flow rate was 400μl/min, injection volume 1 μl. Mass spectrometry was performed using a

6540 QTOF/MS Detector and an AJS ESI source (Agilent, Santa Clara, USA). The measured metabolite intensities were normalized to internal standards.

Glucose uptake assay. After 0, 0.5, 1, or 2 h post-infection, RPMI medium containing glucose was replaced with medium without glucose supplemented with 10 μM of the fluorescent glucose analog 2-NBDG (Life Technologies). After 30 min of incubation at 37˚C, cells were washed with PBS and resuspended in 1% formaldehyde for FACS analysis. FACS Canto (BD biosciences) flow cytometer was used for the acquisition of samples and Flowjo software (Flowjo LLC) was used for data analysis.

Extracellular acidification rate measurement (Seahorse). Extracellular acidification rate (ECAR) was analyzed using a XF96 Extracellular Flux Analyzer (Seahorse Bioscience). BMDMs were infected with *S*. Typhimurium with a MOI of 10 plated in non-buffered media. Measurements were obtained under basal conditions.

Phagosomal β-galactosidase activity assay. To assess the β-galactosidase activity in phagolysosomes, red fluorescent beads (Bangs Laboratories) were coated with 5-Dodecanoylaminofluorescein Di-β-D-Galactopyranoside (C_{12}FDG, Life Technologies) for 60 min at 37˚C in $NaHCO_3$ pH 9.6 buffer. 100 beads per cell were added to BMDMs and incubated for 10 min at RT and 10 min at 37˚C, followed by washings with RPMI to remove extracellular beads. After 0h, 0.5h, 1h or 2h, cells were washed with cold PBS and resuspended in 1% formaldehyde. Samples were acquired in a FACSCanto flow cytometer and Flowjo software. Mean fluorescence intensity (MFI) of C_{12}FDG was normalized to the red MFI of the beads for every sample.

Phagosomal proteolytic activity assay. To assess proteolytic activity in the phagolysosomes, red fluorescent beads were coated with green DQ-BSA (Life Technologies) dissolved in carbodiimide solution (25 mg/mL in PBS) for 30 min at RT. After washing, beads were resuspended in 0.1 M sodium tetraborate decahydrate solution (pH: 8.0 in ddH_2O) and incubated overnight at RT. Beads were then washed, resuspended in RPMI, and added to BMDMs at 100beads/cell. After 10min incubation at RT and 10min incubation at 37˚C, cells were washed to remove non-internalized beads. After 0, 0.5, 1 or 2h, cells were washed with cold PBS and resuspended in 1% formaldehyde. Samples were acquired using a BD FACSCanto flow cytometer and Flowjo software. DQ-BSA MFI was normalized to the red MFI of beads for every sample.

Phagosomal acidification. Phagosome acidification was analyzed using the pH-sensitive fluorescent pHrodo Green conjugated *E. coli* Bioparticles (Life Technologies). These particles were first coated with the pH-insensitive dye Alexa Fluor-647 (Life Technologies) for 1 h at 37˚C in 0.1M sodium tetra borate decahydrate (pH: 8.0 in ddH_2O). Beads were then washed, resuspended in RPMI with 10% FBS and added to the cells (100 bioparticles per sample). After 10 min incubation at RT and 10 min incubation at 37˚C, cells were washed to remove non-internalized bioparticles. After 0h, 0.5h, 1h or 2h, cells were washed with cold PBS and resuspended in 1% formaldehyde. Fluorescent signal was analyzed using a FACSCanto flow cytometer and Flowjo software. pHrodo MFI was normalized to the Alexa-647 MFI for every sample.

Antigen presentation assay. Treated BMDMs were incubated with Fc receptor blocking reagent TruStain fcX (Biolegend) for 5 min on ice and then incubated for 30 min on ice with an antibody specific for MHC class II (I-Ab-PE/Cy7 from Biolegend, cat. Number 116419) or $OVA_{323-339}$-MHC II complexes (TCR-PE/Cy7 from Biolegend, cat. Number 118515) in PBS with 3% FBS solution. After washing, cells were resuspended in 1% formaldehyde in PBS, and samples were acquired using a BD FACSCanto flow cytometer and analyzed using Flowjo software.

OVA processing assay. Octadecyl C18 1μm magnetic beads (SiMAG, Chemicell) were coated with Alexa647-OVA (Life Technologies) in acetate buffer pH: 5.0 for 2 h at RT. After

washing, beads were added to treated or infected BMDMs with a ratio of 300 beads per cell. After 24 h, cells were lysed, and Alexa647-OVA-coated magnetic beads were extracted as described above for the isolation of bead phagosomes. Isolated phagosomes were then resuspended in 1% formaldehyde (in PBS) and Alexa647-OVA signal was acquired and analyzed using a FACSCanto flow cytometer and Flowjo software respectively.

Isolation of bead-containing phagosomes. BMDMs were incubated with Octadecyl C18 1 μm magnetic beads (SiMAG, Chemicell; 300 beads per cell) for 10 min at RT and for 10 min at 37˚C. At each time point, cells were washed with PBS and Equilibration buffer (50 mM PIPES pH: 7.0, 50 mM $MgCl_2$, 5 mM EGTA, 1 mM DTT, 10 μM cytochalasin and protease/phosphatase inhibitor cocktail) was added. Cells were incubated on ice for 20 min and samples were lysed (50 mM PIPES pH: 7.0, 50 mM $MgCl_2$, 5 mM EGTA and 68mM sucrose). Cells were scrapped out and passed through a 26G needle at least 15 times. Bead-containing phagosomes were then separated from the lysate using a magnet.

Isolation of *S*. Typhimurium-containing phagosomes. *S*. Typhimurium-containing phagosomes were isolated as described before [66]. *S*. Typhimurium was grown in BHI broth until OD_{600}:1 and then biotinylated with EZ-link NHS-Biotin reagent (Thermo Fisher Scientific). After washing, biotinylated bacteria were incubated with siMAG Streptavidin ferrofluid (Chemicell). Biotinylated *S*. Typhimurium bound to the Streptavidin ferrofluid was then separated using a magnet and bacteria were quantified using BHI agar plates. Subsequently, BMDMs were infected with biotinylated *S*. Typhimurium bound to the Streptavidin ferrofluid at an MOI of 10. At each time point, *S*. Typhimurium-containing phagosomes were isolated using equilibration and lysis buffer as described for bead-containing phagosome isolation.

***In vitro* bacterial burden and ELISA.** After 0 and 24h post-infection, BMDMs were lysed with 1% Triton X-100, 0.01% SDS in PBS. Several dilutions of the lysate were plated on BHI plates and incubated over night at 37˚C. Next day, *S*. Typhimurium colony forming units (CFU) were enumerated. Supernatants were collected and analyzed for IL-6 and TNFα secretion using ELISA kit (R&D) according to the manufacturer's instructions.

Estimation of bacterial burden *in vivo*. Mice were infected with 100 CFU of *S*. Typhimuirum per mouse by i.v. injection. After 3 days of infection mice were euthanized according to current ethical protocols. Liver was isolated and homogenized using gentleMACS Dissociator (Miltenyi Biotec) in sterile PBS. Extracts of the homogenized livers were plated on BHI Agar plates. After 24 h incubation at 37˚C, bacterial colonies were enumerated. Number of colonies was normalized to per gram of tissue. Mice were injected with 4-OHT intraperitoneally one day before the infection with *S*. Typhimurium and every day during the course of infection until the mice were sacrificed for analysis.

Immunoblot analysis. BMDMs were lysed in RIPA buffer supplemented with 1X protease/phosphatase inhibitor cocktail (Thermo Fisher Scientific). Protein was estimated using Pierce BCA Protein Assay Kit (Thermo Fisher Scientific) according to the manufacturer's instructions. Equal amount of proteins was separated in 10% or 12% SDS-PAGE gels. Proteins were then transferred onto a PVDF membrane and probed with antibodies against Glut1 (sc-7903, Santa Cruz Biotechnology), Enolase (sc-31859, Santa Cruz Biotechnology), HKX-2 (sc-6521, Santa Cruz Biotechnology), v-ATPase A1 (V_0 subunit, sc-28801, Santa Cruz Biotechnology), v-ATPase b1/2 (V_1 subunit, sc-21209, Santa Cruz Biotechnology), H2-I/Abβ (sc-71201, Santa Cruz Biotechnology), phospho-p38 (#9216, Cell Signaling), p38 (#9212, Cell Signaling), phospho-p65 (#3033, Cell Signaling), p65 (#4764, Cell Signaling), HIF1α (NB100-105, Abcam), MondoA (SAB2104303, Sigma-Aldrich), calnexin (sc-11397, Santa Cruz Biotechnology) or β-actin (sc-47778, Santa Cruz Biotechnology). Either calnexin or β-actin was used as loading control. After incubation with secondary HRP-conjugated antibody (R&D) blots were developed using ECL reagent (GE Healthcare).

Immunoprecipitation and Native PAGE. Bead phagosomes were isolated from 2-DG-pre-treated BMDMs as described above and were lysed with radio-immunoprecipitation assay (RIPA) buffer containing protease and phosphatase inhibitors. After preclearing the cell lysate with protein A/G agarose magnetic beads (#16–663, Millipore) for 1 h, beads were removed by placing the tube on a magnetic rack. The whole cell lysate (approximately 500 μg of protein) was incubated with 4 μg of an antibody against V_0 subunit-*a* overnight at 4˚C. A separate sample was incubated with IgG which served as a control. Protein A/G agarose beads were added again and incubated for an additional 1 h at room temperature. The immunoprecipitated proteins along with the agarose beads were collected by placing the tube on a magnetic rack. The collected beads were washed several times with RIPA buffer. The washed samples were mixed with SDS-PAGE sample loading buffer, boiled and resolved on a 10% SDS-polyacrylamide gel. V_1 subunit B immunoprecipitated along with V_0 was identified by Western blot analysis.

To perform Native-PAGE, equal amounts of total protein per sample were mixed with NativePAGE Sample Buffer (Life Technologies) and Triton X-100 (final concentration of 0.5%). Sample proteins were separated according to their masses on a 3.5 to 16% linear gradient acrylamide gel by electrophoresis. After separation, proteins were transferred to a PVDF membrane. Following blocking, membrane was incubated with antibodies directed against the cytosolic subunit of the v-ATPase (anti-vATPase-V_1 subunit B) or against the membrane subunit of the v-ATPase (anti-vATPase-V_0 subunit *a*).

Site-directed mutagenesis. Flag-tagged and catalytically inactive Aldolase A mutant (K147A) was generated using Q5 Site-Directed Mutagenesis Kit from NEB according to the manufacturer's instructions. Constructs were transfected into 293T cells and immunoprecipitation with Flag antibodies was performed.

siRNA Knock down. BMDMs (day 7–9) were seeded between 1-2x10^6 onto a 6 well plate and allowed to settle down overnight. The next day the cells were transfected with 100nM siRNA specific for aldolase A (5′GGAAGAAGGAGAACCUGAA dTdT) or Non-targeting siRNA #1 (D-001810-01-05) from Dharmacon using Lipofectamine 3000 (Life Technologies) or GenMute siRNA Transfection Reagent (SignaGen Laboratories) according to the manufacturer's instructions. Samples were proceeded further for the treatment of infection 48h after transfection incubated with Alexa647-coated pHrodo *E. coli* particles for the analysis of phagosome acidification or infected with *S*. Typhimurium for estimating intracellular bacterial load.

Proximity Ligation Assay (PLA). Interaction between v-ATPase V0 subunit a and v-ATPase V1 subunit B or between aldolase A and v-ATPase V0 a subunit was analyzed using Duolink In Situ PLA (Sigma Aldrich). For the 2-DG experiments, BMDMs were first incubated with 1mM 2-DG for 2h at 37˚C and then fed with magnetic beads (50 beads/cell). Bead-containing cells were incubated for 10min on ice and for 10min at 37˚C. Then non-internalized beads were removed and RPMI supplemented with 10%FBS was added to the cells. Two hours after bead internalization, cells were fixed with 4% formaldehyde at RT for 20 min. For the infection experiments, BMDMs were infected with *S*. Typhimurium as above described. The cells were fixed with 4%formaldehyde for 20min at RT at 30min and 4h post-infection infection. Fixation with formaldehyde was stopped by intensive washing with PBS. Samples were permeabilized with 0.3% Triton X-100 in PBS for 5min and blocked with 5% (w/v) normal goat serum (Life Technologies) in PBS solution. Samples were incubated at 4˚C overnight (O/N) in a humidity chamber with primary antibodies against v-ATPase V0 subunit an (sc-28801, Santa Cruz Biotechnology), v-ATPase V1 subunit B (sc-21209, Santa Cruz Biotechnology) and aldolase A (sc-390733, Santa Cruz Biotechnology) prepared in blocking solution. The next day, samples were washed with 0.03% Triton X-100 in PBS and incubated with DuoLink PLA Probes PLUS and MINUS for 1h at 37˚C. Samples were then washed with DuoLink washing buffer A and incubated with the ligation-ligase solution for 30min at 37˚C. Then samples

were washed again with DuoLink washing buffer A and incubated with an amplification solution containing polymerase for 100min at 37˚C. Finally, samples were washed with DuoLink washing buffer B and mounted onto cover slides with DuoLink DAPI-containing mounting solution for microscopy analysis.

Statistical analysis. Statistical analysis was performed using Graphpad Prism software. Two-tailed Student's *t*-test was conducted for most of the datasets unless specified otherwise to determine statistical significance. All data are represented as mean ± SEM as indicated. For all tests, p-values <0.05 was considered statistically significant ($^{*}p<0.05$; $^{**}p<0.01$; $^{***}p<0.005$).

Supporting information

S1 Fig. related to Fig 1: *S.* Typhimurium infection promotes metabolic reprogramming in macrophages. (**A**) Partial least squares discriminate analysis (PLS-DA) score plot representing the differential metabolomics profiles upon *S.* Typhimurium infection (*S.*T., 2h p.i.) compared to uninfected controls (n = 6). (**B**) Heatmap representation of 2-way hierarchical clustering of all altered metabolites analyzed from BMDMs upon *S.* Typhimurium infection (2h p.i.) compared to uninfected controls (n = 6). (**C**) Relative quantification of NAD^{+}/NADH ratio of uninfected (UI) and *S.* Typhimurium-infected BMDMs (S.T., 1h and 4h p.i.) by targeted MS-UPLC analysis (n = 6). (**D**) Hierarchical clustering of the major differentially regulated transcripts in BMDMs infected with *S.* Typhimurium (2h p.i) compared to uninfected controls (n = 3). (**E**) Western blot analysis of insulin receptor and its downstream effector phospho-GSK3β; calnexin was used as a loading control. **(F)** Expression of insulin receptor was quantified from immunoblots using ImageJ and its relative expression to loading control is shown (n = 4). Data are shown as mean ± S.E.M. and statistical significance calculated using student t-test is represented as * = $p<0.05$; ** = $p<0.01$; *** = $p<0.001$.
(TIF)

S2 Fig. related to Fig 2: Virulence dependent inhibition of glycolysis in *S.* Typhimurium infected macrophages. (**A**) Relative quantification of UDP-glucose, ribose-5-phosphate and succinate levels in *S.* Typhimurium-infected BMDMs (2h p.i.) by targeted MS-UPLC analysis (n = 6). (**B**) Cytotoxicity of *S.* Typhimurium towards BMDMs was determined by measuring lactate dehydrogenase (LDH) in the cell supernatant at 1 and 4h post-infection. (**C**) Expression levels of the glycolytic genes detected in the RNA-seq analysis represented a fold increase upon *S.* Typhimurium infection relative to uninfected controls (UI). (**D**) Glucose intake in *S.* Typhimurium-infected BMDMs (S.T.) and heat-killed *S.* Typhimurium-treated BMDMs (HK S.T.) **(E)** WT, ssrB and invA mutant *S.* Typhimurium for 2h represented as the fold increase in 2-NBDG MFI relative to uninfected (UI) controls analyzed by flow cytometry (n = 6). Data are shown as mean ± S.E.M. and statistical significance calculated using student t-test is represented as * = $p<0.05$; ** = $p<0.01$; *** = $p<0.001$. **(F)** Bacterial intake of WT and *invA* mutant *S.* Typhimurium in BMDMs measured by colony counting assay. The time point Zero, i.e immediately after washing off extracellular bacteria was used.
(TIF)

S3 Fig. related to Fig 3: Macrophages depend on glycolysis for the clearance of intracellular bacteria. (A) Quantification of intracellular *S.* Typhimurium burden at 24h post-infection in untreated (UT) and fasentin-treated BMDMs (n = 3) **(B)** BMDMs grown in Glucose Free Medium (GFM) (n = 3). **(C)** *S.* Typhimurium burden in BMDMs pre-treated with 2-DG or Sodium pyruvate or both were represented as colony forming units (CFU) 24h post-infection. **(D)** Luminiusence of 2-DG and sodium pyruvate **(E)** oligomycin were analyzed using Promega CellTiter-Glo luminescent assay **(F)** *S.* Typhimurium burden in BMDMs from

oligomycin treated BMDMs analyzed 24h post-infection. **(G)** Glucose uptake in WT and $IR^{\Delta myel}$ BMDMs measured as 2-NBDG mean fluorescence intensity (MFI) by flow cytometry (n = 3). **(H)** Western blot analysis of Glut1 expression from WT and IR KO BMDMs at the indicated time points. The image shown is representative of 3 individual experiments **(I)** Intracellular *S*. Typhimurium levels in UT and recombinant insulin pre-treated BMDMs 24h post-infection.
(TIF)

S4 Fig. related to Fig 3: Macrophages depend on glycolysis for the clearance of intracellular bacteria. (**A**) Glucose uptake in *S*. Typhimurium-infected and 4-OHT-treated BMDMs compared to infected and untreated controls (UT) measured as 2-NBDG MFI by flow cytometry (n = 3). 2-NBDG was acquired at 2h post-infection. Data is normalized to uninfected controls. (**B**) Sea Horse measurement of ECAR in 4-OHT-treated BMDMs compared to untreated controls (n = 6). (**C**) Quantification of intracellular *S*. Typhimurium burden at 24h post-infection in untreated (UT) BMDMs compared to BMDMs simultaneously treated with 2-DG and 4-OHT (n = 3). **(D)** Growth curves of *S*. Typhimurium measure at ID_{600} in the presence of 2-DG or 4-OHT in LB medium supplemented with streptomycin. **(E)** IL-6 and TNF-α secretion by 2-DG-treated macrophages infected with *S*. Typhimurium (**F**), *L*. *monocytogenes* (**G**) or *S*. *aureus* represented 24h post-infection. **(H)** IL-6 and TNF-α levels measured from macrophages infected with *S*. Typhimurium in Glucose Free Medium **(I)** IL-6 and TNFα in supernatants of $IR^{\Delta myel}$ BMDMs and WT infected with *S*. Typhimurium for 24h (n = 3). (**J**) IL-6 and TNFα in supernatants from 4-OHT-treated BMDMs after 24h of infection with *S*. Typhimurium (n = 3). (**K**) Western blot analysis of phospho-p65 and phospho-p38 in 2-DG-pre-treated and *S*. Typhimurium-infected BMDMs compared to untreated (UT) controls. The image shown is representative of 3 individual experiments. (**L**) MFI of unprocessed Alexa647-labelled OVA in bead containing phagosomes from 4-OHT-treated and *S*. Typhimurium-infected BMDMs analyzed by flow cytometry (n = 3). Data are shown as mean ± S.E.M. and statistical significance calculated using student t-test is represented as * = $p<0.05$; ** = $p<0.01$; *** = $p<0.001$.
(TIF)

S5 Fig. related to Fig 4: Glycolysis is crucial for phagosome maturation upon infection in macrophages. (**A**) Intake of fluorescent beads (APC) by WT and $IR^{\Delta myel}$ BMDMs shown as mean fluorescent intensity (MFI) analyzed by flow cytometry (n = 3). (**B**) Intake of fluorescent beads in 2-DG-treated BMDMs compared to untreated BMDMs analyzed by flow cytometry and shown as MFI (n = 3). (**C**) Flow cytometry analysis of C_{12}FDG and Alexa647-coated beads in *S*. Typhimurium-infected BMDMs for 30min compared to uninfected (UI) BMDMs (MFI of C_{12}FDG normalized to Alexa647 MFI) (n = 3). Data are shown as mean ± S.E.M. and statistical significance calculated using student t-test is represented as * = $p<0.05$; ** = $p<0.01$; *** = $p<0.001$.
(TIF)

S6 Fig. related to Fig 5: Glycolysis critically regulates the acidification of phagosome and the assembly of v-ATPase complex. (A) MFI of pHrodo-*E*. *coli* particles in *S*. Typhimurium infected WT BMDMs grown in Glucose-free medium **(B)** MFI of pHrodo-*E*. *coli* particles in WT, *ΔinvA*, *ΔssrB* mutant *S*. Typhimurium infected BMDMs and 4-OHT treated BMDMs infected with *S*. Typhimurium (2h p.i.) normalized to Alexa647 MFI (n = 3). (**C**) Western blot analysis of v-ATPase subunits V_0 and V_1 in isolated phagosomes from fasentin-treated BMDMs. The image shown is representative of 3 individual experiments. (**D**) Western blot analysis of total levels of the v-ATPase subunits V_0 and V_1 in 2-DG-treated-BMDMs. The

image shown is representative of 3 individual experiments. (**E**) Western blot analysis of total levels of the v-ATPase subunits V_0 and V_1 in fasentin-treated-BMDMs. (**F**) PLA analysis of v-ATPase subunits V_0 and V_1 interaction in 2-DG-treated BMDMs infected with *S*. Typhimurium using confocal microscopy (scale bars indicate 10 μm). The image shown is representative of 3 individual experiments. (**G**) Quantification of V_0 and V_1 interaction in 2-DG treated BMDMs (n = 15). Data are shown as mean ± S.E.M. and statistical significance calculated using student t-test is represented as * = $p<0.05$; ** = $p<0.01$; *** = $p<0.001$.
(TIF)

S7 Fig. related to Fig 5: Glycolysis critically regulates the acidification of phagosome and the assembly of v-ATPase complex. (A) Immunoprecipitation of V0 subunit from isolated bead phagosomes grown in glucose-free medium analyzed for V0 and V1 subunits. **(B)** Native PAGE analysis of isolated bead phagosome from BMDMs grown in Glucose free medium (GFM).
(TIF)

S8 Fig. related to Fig 6: Aldolase A critically regulates the assembly of v-ATPase and phagosome acidification. (A) Immunoblot from isolated *S*. Typhimurium phagosomes probed for Aldolase A and phosphofructokinase (PFK) and actin at indicated time points.
(TIF)

S1 Table. List of isotopically labelled internal standards and their concentrations used for metabolite analysis.
(PDF)

Acknowledgments

We thank Adam Antebi, Max Planck Institute for the Biology of Ageing for critically reading the manuscript and Jens Bruning, Max Planck Institute for Metabolism Research for providing us the $IR^{\Delta myel}$ mice. Graphical abstract was created using Biorender.

Author Contributions

Conceptualization: Saray Gutiérrez, Nirmal Robinson.

Data curation: Saray Gutiérrez, Peter Frommolt, Vidya Velagapudi.

Formal analysis: Saray Gutiérrez, Julia Fischer, Raja Ganesan, Martina Wolke, Alberto Pessia.

Funding acquisition: Nina Judith Hos, Nirmal Robinson.

Investigation: Saray Gutiérrez, Julia Fischer, Nina Judith Hos, Gökhan Cildir, Martina Wolke, Alberto Pessia, Vincenzo Desiderio, Vidya Velagapudi, Nirmal Robinson.

Methodology: Saray Gutiérrez, Julia Fischer, Raja Ganesan, Gökhan Cildir, Martina Wolke, Alberto Pessia, Vidya Velagapudi.

Project administration: Nirmal Robinson.

Resources: Nirmal Robinson.

Software: Peter Frommolt.

Supervision: Peter Frommolt, Vidya Velagapudi, Nirmal Robinson.

Validation: Vincenzo Desiderio.

Visualization: Peter Frommolt.

Writing – original draft: Saray Gutiérrez, Raja Ganesan, Vidya Velagapudi, Nirmal Robinson.

Writing – review & editing: Saray Gutiérrez, Gökhan Cildir, Vincenzo Desiderio, Nirmal Robinson.

References

1. Ginhoux F, Schultze JL, Murray PJ, Ochando J, Biswas SK. New insights into the multidimensional concept of macrophage ontogeny, activation and function. Nat Immunol. 2016; 17(1):34–40. https://doi.org/10.1038/ni.3324 PMID: 26681460.
2. Robinson N, McComb S, Mulligan R, Dudani R, Krishnan L, Sad S. Type I interferon induces necroptosis in macrophages during infection with Salmonella enterica serovar Typhimurium. Nature immunology. 2012; 13(10):954–62. Epub 2012/08/28. https://doi.org/10.1038/ni.2397 PMID: 22922364; PubMed Central PMCID: PMC4005791.
3. Zhang DW, Shao J, Lin J, Zhang N, Lu BJ, Lin SC, et al. RIP3, an energy metabolism regulator that switches TNF-induced cell death from apoptosis to necrosis. Science. 2009; 325(5938):332–6. Epub 2009/06/06. https://doi.org/10.1126/science.1172308 PMID: 19498109.
4. Delmastro-Greenwood MM, Piganelli JD. Changing the energy of an immune response. Am J Clin Exp Immunol. 2013; 2(1):30–54. Epub 2013/07/26. PMID: 23885324; PubMed Central PMCID: PMC3714201.
5. Krawczyk CM, Holowka T, Sun J, Blagih J, Amiel E, DeBerardinis RJ, et al. Toll-like receptor-induced changes in glycolytic metabolism regulate dendritic cell activation. Blood. 2010; 115(23):4742–9. https://doi.org/10.1182/blood-2009-10-249540 ISI:000278635900021. PMID: 20351312
6. Galvan-Pena S, O'Neill LA. Metabolic reprograming in macrophage polarization. Front Immunol. 2014; 5:420. Epub 2014/09/18. https://doi.org/10.3389/fimmu.2014.00420 PMID: 25228902; PubMed Central PMCID: PMC4151090.
7. Rodriguez-Prados JC, Traves PG, Cuenca J, Rico D, Aragones J, Martin-Sanz P, et al. Substrate Fate in Activated Macrophages: A Comparison between Innate, Classic, and Alternative Activation. J Immunol. 2010; 185(1):605–14. https://doi.org/10.4049/jimmunol.0901698 ISI:000278933800066. PMID: 20498354
8. Huang SCC, Everts B, Ivanova Y, O'Sullivan D, Nascimento M, Smith AM, et al. Cell-intrinsic lysosomal lipolysis is essential for alternative activation of macrophages. Nat Immunol. 2014; 15(9):846–55. https://doi.org/10.1038/ni.2956 ISI:000340739400012. PMID: 25086775
9. Kornberg MD, Bhargava P, Kim PM, Putluri V, Snowman AM, Putluri N, et al. Dimethyl fumarate targets GAPDH and aerobic glycolysis to modulate immunity. Science. 2018; 360(6387):449–53. https://doi.org/10.1126/science.aan4665 PMID: 29599194; PubMed Central PMCID: PMC5924419.
10. Mills EL, Ryan DG, Prag HA, Dikovskaya D, Menon D, Zaslona Z, et al. Itaconate is an anti-inflammatory metabolite that activates Nrf2 via alkylation of KEAP1. Nature. 2018; 556(7699):113–7. https://doi.org/10.1038/nature25986 PMID: 29590092.
11. Tannahill GM, Curtis AM, Adamik J, Palsson-McDermott EM, McGettrick AF, Goel G, et al. Succinate is an inflammatory signal that induces IL-1 beta through HIF-1 alpha. Nature. 2013; 496(7444):238–+. https://doi.org/10.1038/nature11986 ISI:000317346300045. PMID: 23535595
12. Eisele NA, Ruby T, Jacobson A, Manzanillo PS, Cox JS, Lam L, et al. Salmonella Require the Fatty Acid Regulator PPAR delta for the Establishment of a Metabolic Environment Essential for Long-Term Persistence. Cell Host Microbe. 2013; 14(2):171–82. https://doi.org/10.1016/j.chom.2013.07.010 ISI:000330851600008. PMID: 23954156
13. Bowden SD, Rowley G, Hinton JC, Thompson A. Glucose and glycolysis are required for the successful infection of macrophages and mice by Salmonella enterica serovar typhimurium. Infect Immun. 2009; 77(7):3117–26. Epub 2009/04/22. https://doi.org/10.1128/IAI.00093-09 PMID: 19380470; PubMed Central PMCID: PMC2708584.
14. Ganesan R, Hos NJ, Gutierrez S, Fischer J, Stepek JM, Daglidu E, et al. Salmonella Typhimurium disrupts Sirt1/AMPK checkpoint control of mTOR to impair autophagy. PLoS pathogens. 2017; 13(2): e1006227. Epub 2017/02/14. https://doi.org/10.1371/journal.ppat.1006227 PMID: 28192515; PubMed Central PMCID: PMC5325604.
15. Fischer J, Gutierrez S, Ganesan R, Calabrese C, Ranjan R, Cildir G, et al. Leptin signaling impairs macrophage defenses against Salmonella Typhimurium. Proceedings of the National Academy of Sciences

of the United States of America. 2019; 116(33):16551–60. Epub 2019/07/28. https://doi.org/10.1073/pnas.1904885116 PMID: 31350351; PubMed Central PMCID: PMC6697794.

16. Galic S, Sachithanandan N, Kay TW, Steinberg GR. Suppressor of cytokine signalling (SOCS) proteins as guardians of inflammatory responses critical for regulating insulin sensitivity. Biochem J. 2014; 461 (2):177–88. Epub 2014/06/27. https://doi.org/10.1042/BJ20140143 PMID: 24966052.

17. Weng LP, Smith WM, Brown JL, Eng C. PTEN inhibits insulin-stimulated MEK/MAPK activation and cell growth by blocking IRS-1 phosphorylation and IRS-1/Grb-2/Sos complex formation in a breast cancer model. Hum Mol Genet. 2001; 10(6):605–16. Epub 2001/03/07. https://doi.org/10.1093/hmg/10.6.605 PMID: 11230180.

18. Kelly B O'Neill LA. Metabolic reprogramming in macrophages and dendritic cells in innate immunity. Cell Res. 2015; 25(7):771–84. Epub 2015/06/06. https://doi.org/10.1038/cr.2015.68 PMID: 26045163; PubMed Central PMCID: PMC4493277.

19. Freemerman AJ, Johnson AR, Sacks GN, Milner JJ, Kirk EL, Troester MA, et al. Metabolic reprogramming of macrophages: glucose transporter 1 (GLUT1)-mediated glucose metabolism drives a proinflammatory phenotype. J Biol Chem. 2014; 289(11):7884–96. Epub 2014/02/05. https://doi.org/10.1074/jbc.M113.522037 PMID: 24492615; PubMed Central PMCID: PMC3953299.

20. Pérez-Morales D, Banda MM, Chau NYE, Salgado H, Martínez-Flores I, Ibarra JA, et al. The transcriptional regulator SsrB is involved in a molecular switch controlling virulence lifestyles of Salmonella. PLoS pathogens. 2017; 13(7):e1006497. https://doi.org/10.1371/journal.ppat.1006497 PMID: 28704543

21. Galán JE, Curtiss 3rd R. Distribution of the invA,-B,-C, and-D genes of Salmonella typhimurium among other Salmonella serovars: invA mutants of Salmonella typhi are deficient for entry into mammalian cells. Infection and immunity. 1991; 59(9):2901–8. https://doi.org/10.1128/iai.59.9.2901-2908.1991 PMID: 1879916

22. Lindgren SW, Stojiljkovic I, Heffron F. Macrophage killing is an essential virulence mechanism of Salmonella typhimurium. Proceedings of the National Academy of Sciences. 1996; 93(9):4197–201. https://doi.org/10.1073/pnas.93.9.4197 PMID: 8633040

23. Mauer J, Chaurasia B, Plum L, Quast T, Hampel B, Bluher M, et al. Myeloid cell-restricted insulin receptor deficiency protects against obesity-induced inflammation and systemic insulin resistance. Plos Genet. 2010; 6(5):e1000938. Epub 2010/05/14. https://doi.org/10.1371/journal.pgen.1000938 PMID: 20463885; PubMed Central PMCID: PMC2865520.

24. Doughty CA, Bleiman BF, Wagner DJ, Dufort FJ, Mataraza JM, Roberts MF, et al. Antigen receptor–mediated changes in glucose metabolism in B lymphocytes: role of phosphatidylinositol 3-kinase signaling in the glycolytic control of growth. Blood. 2006; 107(11):4458–65. https://doi.org/10.1182/blood-2005-12-4788 PMID: 16449529

25. Daurio NA, Tuttle SW, Worth AJ, Song EY, Davis JM, Snyder NW, et al. AMPK Activation and Metabolic Reprogramming by Tamoxifen through Estrogen Receptor–Independent Mechanisms Suggests New Uses for This Therapeutic Modality in Cancer Treatment. Cancer Research. 2016; 76(11):3295–306. https://doi.org/10.1158/0008-5472.CAN-15-2197 PMID: 27020861

26. Lennon-Dumenil AM, Bakker AH, Maehr R, Fiebiger E, Overkleeft HS, Rosemblatt M, et al. Analysis of protease activity in live antigen-presenting cells shows regulation of the phagosomal proteolytic contents during dendritic cell activation. J Exp Med. 2002; 196(4):529–40. Epub 2002/08/21. https://doi.org/10.1084/jem.20020327 PMID: 12186844; PubMed Central PMCID: PMC2196045.

27. Forgac M. Vacuolar ATPases: rotary proton pumps in physiology and pathophysiology. Nat Rev Mol Cell Biol. 2007; 8(11):917–29. Epub 2007/10/04. https://doi.org/10.1038/nrm2272 PMID: 17912264.

28. Kane PM. Disassembly and reassembly of the yeast vacuolar H(+)-ATPase in vivo. J Biol Chem. 1995; 270(28):17025–32. Epub 1995/07/14. PMID: 7622524.

29. Lu M, Sautin YY, Holliday LS, Gluck SL. The glycolytic enzyme aldolase mediates assembly, expression, and activity of vacuolar H+-ATPase. The Journal of biological chemistry. 2004; 279(10):8732–9. Epub 2003/12/16. https://doi.org/10.1074/jbc.M303871200 PMID: 14672945.

30. Su Y, Zhou A, Al-Lamki RS, Karet FE. The a-subunit of the V-type H+-ATPase interacts with phosphofructokinase-1 in humans. The Journal of biological chemistry. 2003; 278(22):20013–8. Epub 2003/03/22. https://doi.org/10.1074/jbc.M210077200 PMID: 12649290.

31. Starnes GL, Coincon M, Sygusch J, Sibley LD. Aldolase is essential for energy production and bridging adhesin-actin cytoskeletal interactions during parasite invasion of host cells. Cell Host Microbe. 2009; 5 (4):353–64. https://doi.org/10.1016/j.chom.2009.03.005 PMID: 19380114; PubMed Central PMCID: PMC2683947.

32. St-Jean M, Blonski C, Sygusch J. Charge stabilization and entropy reduction of central lysine residues in fructose-bisphosphate aldolase. Biochemistry. 2009; 48(21):4528–37. https://doi.org/10.1021/bi8021558 PMID: 19354220.

33. O'Neill LA, Pearce EJ. Immunometabolism governs dendritic cell and macrophage function. J Exp Med. 2016; 213(1):15–23. Epub 2015/12/24. https://doi.org/10.1084/jem.20151570 PMID: 26694970; PubMed Central PMCID: PMC4710204.

34. Mehrotra P, Jamwal SV, Saquib NM, Sinha N, Siddiqui Z, Manivel V, et al. Pathogenicity of Mycobacterium tuberculosis Is Expressed by Regulating Metabolic Thresholds of the Host Macrophage. Plos Pathog. 2014; 10(7). ARTN e1004265 https://doi.org/10.1371/journal.ppat.1004265 ISI:000340551000045. PMID: 25058590

35. Hernandez LD, Pypaert M, Flavell RA, Galan JE. A Salmonella protein causes macrophage cell death by inducing autophagy. J Cell Biol. 2003; 163(5):1123–31. https://doi.org/10.1083/jcb.200309161 ISI:000187430500018. PMID: 14662750

36. Layton AN, Brown PJ, Galyov EE. The Salmonella translocated effector SopA is targeted to the mitochondria of infected cells. J Bacteriol. 2005; 187(10):3565–71. Epub 2005/05/04. https://doi.org/10.1128/JB.187.10.3565-3571.2005 PMID: 15866946; PubMed Central PMCID: PMC1112013.

37. Hos NJ, Ganesan R, Gutierrez S, Hos D, Klimek J, Abdullah Z, et al. Type I interferon enhances necroptosis of Salmonella Typhimurium-infected macrophages by impairing antioxidative stress responses. The Journal of cell biology. 2017; 216(12):4107–21. Epub 2017/10/22. https://doi.org/10.1083/jcb.201701107 PMID: 29055012; PubMed Central PMCID: PMC5716270.

38. Liu XY, Lu R, Xia YL, Sun J. Global analysis of the eukaryotic pathways and networks regulated by Salmonella typhimurium in mouse intestinal infection in vivo. Bmc Genomics. 2010;11. Artn 722 https://doi.org/10.1186/1471-2164-11-11 ISI:000286246800001. PMID: 20053297

39. Antunes LCM, Arena ET, Menendez A, Han J, Ferreira RBR, Buckner MMC, et al. Impact of Salmonella Infection on Host Hormone Metabolism Revealed by Metabolomics. Infect Immun. 2011; 79(4):1759–69. https://doi.org/10.1128/IAI.01373-10 ISI:000288532300039. PMID: 21321075

40. Jiang L, Wang P, Song X, Zhang H, Ma S, Wang J, et al. Salmonella Typhimurium reprograms macrophage metabolism via T3SS effector SopE2 to promote intracellular replication and virulence. Nature communications. 2021; 12(1). https://doi.org/10.1038/s41467-021-21186-4 PMID: 33563986

41. Ding K, Zhang C, Li J, Chen S, Liao C, Cheng X, et al. cAMP Receptor Protein of Salmonella enterica Serovar Typhimurium Modulate Glycolysis in Macrophages to Induce Cell Apoptosis. Current Microbiology. 2019; 76(1):1–6. https://doi.org/10.1007/s00284-018-1574-1 PMID: 30315323

42. Sanman LE, Qian Y, Eisele NA, Ng TM, Van Der Linden WA, Monack DM, et al. Disruption of glycolytic flux is a signal for inflammasome signaling and pyroptotic cell death. eLife. 2016;5. https://doi.org/10.7554/eLife.13663 PMID: 27011353; PubMed Central PMCID: PMC4846378.

43. Everts B, Amiel E, Huang SCC, Smith AM, Chang CH, Lam WY, et al. TLR-driven early glycolytic reprogramming via the kinases TBK1-IKK epsilon supports the anabolic demands of dendritic cell activation. Nat Immunol. 2014; 15(4):323–+. https://doi.org/10.1038/ni.2833 ISI:000333252000007. PMID: 24562310

44. Lambeth JD. NOX enzymes and the biology of reactive oxygen. Nat Rev Immunol. 2004; 4(3):181–9. Epub 2004/03/25. https://doi.org/10.1038/nri1312 PMID: 15039755.

45. Buchmeier NA, Heffron F. Inhibition of Macrophage Phagosome-Lysosome Fusion by Salmonella-Typhimurium. Infect Immun. 1991; 59(7):2232–8. ISI:A1991FT92200002. https://doi.org/10.1128/iai.59.7.2232-2238.1991 PMID: 2050395

46. Oh YK, AlpucheAranda C, Berthiaume E, Jinks T, Miller SI, Swanson JA. Rapid and complete fusion of macrophage lysosomes with phagosomes containing Salmonella typhimurium. Infect Immun. 1996; 64(9):3877–83. ISI:A1996VE44300061. https://doi.org/10.1128/iai.64.9.3877-3883.1996 PMID: 8751942

47. Mills SD, Finlay BB. Isolation and characterization of Salmonella typhimurium and Yersinia pseudotuberculosis-containing phagosomes from infected mouse macrophages: Y-pseudotuberculosis traffics to terminal lysosomes where they are degraded. Eur J Cell Biol. 1998; 77(1):35–47. ISI:000076446400005. https://doi.org/10.1016/S0171-9335(98)80100-3 PMID: 9808287

48. Coombes BK, Brown NF, Valdez Y, Brumell JH, Finlay BB. Expression and secretion of Salmonella pathogenicity island-2 virulence genes in response to acidification exhibit differential requirements of a functional type III secretion apparatus and SsaL. Journal of Biological Chemistry. 2004; 279(48):49804–15. https://doi.org/10.1074/jbc.M404299200 ISI:000225229500033. PMID: 15383528

49. Albaghdadi H, Robinson N, Finlay B, Krishnan L, Sad S. Selectively reduced intracellular proliferation of Salmonella enterica serovar typhimurium within APCs limits antigen presentation and development of a rapid CD8 T cell response. J Immunol. 2009; 183(6):3778–87. Epub 2009/08/21. https://doi.org/10.4049/jimmunol.0900843 PMID: 19692639; PubMed Central PMCID: PMC4011801.

50. Lisec J, Schauer N, Kopka J, Willmitzer L, Fernie AR. Gas chromatography mass spectrometry-based metabolite profiling in plants. Nat Protoc. 2006; 1(1):387–96. Epub 2007/04/05. https://doi.org/10.1038/nprot.2006.59 PMID: 17406261.

51. Vieira OV, Botelho RJ, Grinstein S. Phagosome maturation: aging gracefully. The Biochemical journal. 2002; 366(Pt 3):689–704. Epub 2002/06/14. https://doi.org/10.1042/BJ20020691 PMID: 12061891; PubMed Central PMCID: PMC1222826.

52. West AP, Brodsky IE, Rahner C, Woo DK, Erdjument-Bromage H, Tempst P, et al. TLR signalling augments macrophage bactericidal activity through mitochondrial ROS. Nature. 2011; 472(7344):476–80. Epub 2011/04/29. https://doi.org/10.1038/nature09973 PMID: 21525932; PubMed Central PMCID: PMC3460538.

53. Chakravortty D, Hensel M. Inducible nitric oxide synthase and control of intracellular bacterial pathogens. Microbes Infect. 2003; 5(7):621–7. https://doi.org/10.1016/s1286-4579(03)00096-0 ISI:000184176900007. PMID: 12787738

54. Sturgillkoszycki S. Lack of Acidification in Mycobacterium Phagosomes Produced by Exclusion of the Vesicular Proton-Atpase (Vol 263, Pg 678, 1994). Science. 1994; 263(5152):1359–. ISI: A1994MZ92700006. https://doi.org/10.1126/science.8128214 PMID: 8128214

55. Nordenfelt P, Grinstein S, Bjorck L, Tapper H. V-ATPase-mediated phagosomal acidification is impaired by Streptococcus pyogenes through Mga-regulated surface proteins. Microbes Infect. 2012; 14 (14):1319–29. https://doi.org/10.1016/j.micinf.2012.08.005 ISI:000312418700011. PMID: 22981599

56. Kohio HP, Adamson AL. Glycolytic control of vacuolar-type ATPase activity: A mechanism to regulate influenza viral infection. Virology. 2013; 444(1–2):301–9. https://doi.org/10.1016/j.virol.2013.06.026 ISI:000323873600035. PMID: 23876457

57. Havula E, Teesalu M, Hyotylainen T, Seppala H, Hasygar K, Auvinen P, et al. Mondo/ChREBP-Mlx-Regulated Transcriptional Network Is Essential for Dietary Sugar Tolerance in Drosophila. Plos Genet. 2013; 9(4). ARTN e1003438 https://doi.org/10.1371/journal.pgen.1003438 ISI:000318073300032. PMID: 23593032

58. Chang CH, Curtis JD, Maggi LB Jr., Faubert B, Villarino AV, O'Sullivan D, et al. Posttranscriptional control of T cell effector function by aerobic glycolysis. Cell. 2013; 153(6):1239–51. Epub 2013/06/12. https://doi.org/10.1016/j.cell.2013.05.016 PMID: 23746840; PubMed Central PMCID: PMC3804311.

59. Schindler A, Foley E. Hexokinase 1 blocks apoptotic signals at the mitochondria. Cell Signal. 2013; 25 (12):2685–92. https://doi.org/10.1016/j.cellsig.2013.08.035 ISI:000328179800035. PMID: 24018046

60. Roman-Garcia P, Quiros-Gonzalez I, Mottram L, Lieben L, Sharan K, Wangwiwatsin A, et al. Vitamin B (1)(2)-dependent taurine synthesis regulates growth and bone mass. J Clin Invest. 2014; 124(7):2988–3002. Epub 2014/06/10. https://doi.org/10.1172/JCI72606 PMID: 24911144; PubMed Central PMCID: PMC4071367.

61. Xia J, Sinelnikov IV, Han B, Wishart DS. MetaboAnalyst 3.0—making metabolomics more meaningful. Nucleic Acids Res. 2015; 43(W1):W251–7. Epub 2015/04/22. https://doi.org/10.1093/nar/gkv380 PMID: 25897128; PubMed Central PMCID: PMC4489235.

62. Wagle P, Nikolic M, Frommolt P. QuickNGS elevates Next-Generation Sequencing data analysis to a new level of automation. Bmc Genomics. 2015; 16:487. Epub 2015/07/02. https://doi.org/10.1186/s12864-015-1695-x PMID: 26126663; PubMed Central PMCID: PMC4486389.

63. Kim D, Pertea G, Trapnell C, Pimentel H, Kelley R, Salzberg SL. TopHat2: accurate alignment of transcriptomes in the presence of insertions, deletions and gene fusions. Genome Biol. 2013; 14(4):R36. Epub 2013/04/27. https://doi.org/10.1186/gb-2013-14-4-r36 PMID: 23618408; PubMed Central PMCID: PMC4053844.

64. Trapnell C, Williams BA, Pertea G, Mortazavi A, Kwan G, van Baren MJ, et al. Transcript assembly and quantification by RNA-Seq reveals unannotated transcripts and isoform switching during cell differentiation. Nat Biotechnol. 2010; 28(5):511–5. Epub 2010/05/04. https://doi.org/10.1038/nbt.1621 PMID: 20436464; PubMed Central PMCID: PMC3146043.

65. Love MI, Huber W, Anders S. Moderated estimation of fold change and dispersion for RNA-seq data with DESeq2. Genome Biol. 2014; 15(12):550. Epub 2014/12/18. https://doi.org/10.1186/s13059-014-0550-8 PMID: 25516281; PubMed Central PMCID: PMC4302049.

66. Gutierrez S, Wolke M, Plum G, Robinson N. Isolation of Salmonella typhimurium-containing Phagosomes from Macrophages. Journal of visualized experiments: JoVE. 2017;(128). Epub 2017/11/21. https://doi.org/10.3791/56514 PMID: 29155747.